POLITECNICO DI TORINO
Repository ISTITUZIONALE

A Review of Experimental Investigations into the Time Evolution of Low-Pressure Capacitively Coupled Plasmas in Their Early Stages of Development

Original
A Review of Experimental Investigations into the Time Evolution of Low-Pressure Capacitively Coupled Plasmas in Their Early Stages of Development / Mandracci, P.. - In: PLASMA. - ISSN 2571-6182. - ELETTRONICO. - 7:3(2024), pp. 531-565. [10.3390/plasma7030029]

Availability:
This version is available at: 11583/2995653 since: 2024-12-19T10:13:54Z

Publisher:
MDPI

Published
DOI:10.3390/plasma7030029

Terms of use:

This article is made available under terms and conditions as specified in the corresponding bibliographic description in the repository

Publisher copyright

(Article begins on next page)

07 October 2026

plasma

MDPI

Review

A Review of Experimental Investigations into the Time Evolution of Low-Pressure Capacitively Coupled Plasmas in Their Early Stages of Development

Pietro Mandracci

Department of Applied Science and Technology, Politecnico di Torino, Corso Duca degli Abruzzi 24, I-10129 Turin, Italy; pietro.mandracci@polito.it

Abstract: Capacitively coupled plasma (CCP) discharges working at low pressure are widely used for the synthesis of thin films and the modification of the surface properties of materials. Due to their importance, considerable research was carried out over the years to understand their working mechanisms, and the physical properties of the CCP discharges were measured by many research groups, while simulations of their characteristics were often performed using both fluid and kinematic models. However, most of the simulation and characterization work found in the literature is focused on the discharge steady-state characteristics, since most of the applications rely on its properties, while less information is available on the early stages. In fact, the initial stages of CCP plasma discharges are of great importance to improve the understanding of their ignition process as well as to figure out the working mechanism of pulsed discharges, the use of which has increased in importance in recent years. In this work, a review of the results published in recent years concerning the physical mechanisms involved in the very first stages of low-pressure CCP discharges is presented, focusing on the first few microseconds of discharge time.

Keywords: CCP; low-pressure plasma; plasma ignition

check for updates

Citation: Mandracci, P. A Review of Experimental Investigations into the Time Evolution of Low-Pressure Capacitively Coupled Plasmas in Their Early Stages of Development. *Plasma* **2024**, *7*, 531–565. https://doi.org/10.3390/plasma7030029

Academic Editor: Demetre J. Economou

Received: 17 May 2024
Revised: 11 July 2024
Accepted: 19 July 2024
Published: 22 July 2024

Copyright: © 2024 by the author. Licensee MDPI, Basel, Switzerland. This article is an open access article distributed under the terms and conditions of the Creative Commons Attribution (CC BY) license (https://creativecommons.org/licenses/by/4.0/).

1. Introduction

Plasma discharges are of great importance in modern technology, especially due to their ability to activate chemical reactions at low temperatures, thanks to the molecular dissociation processes that can be activated by high-energy electrons [1]. Thin-film deposition and surface modification processes [2] used in microelectronics [3] are a typical example of the technological application of plasma discharges, but these techniques are also used in several other fields, such as photovoltaics, ref. [4] production of materials for energy-saving applications, ref. [5] pollution control, ref. [6] as well as biomedicine. Ref. [7] Low-pressure discharges have been used for a much longer time compared with atmospheric pressure ones since a lower power density is required for their activation and they allow simpler control of the process parameters. Ref. [1] Among them, radio frequency-activated capacitively coupled plasma discharges (RF-CCP) are of especially widespread use, thanks to their simplicity and relatively low cost, compared with other discharge types, such as inductively coupled plasmas (ICP) or microwave-activated ones [8].

Due to their high technological interest, low-pressure RF-CCP discharges have been widely studied, both theoretically and experimentally, and a considerable amount of literature can be found about them [9]. However, most of the studies are focused on the behavior of plasma when the steady state has been reached, and all the parameters have assumed approximately constant values. In fact, most technological processes that make use of plasma discharges work at the steady state, since it is usually desirable to have stable values of parameters such as deposition rate or etching rate. For these reasons, a relatively low amount of information is available about the discharge behavior during the transition time that is required to reach the steady state, or the time evolution of the plasma

parameters during a cycle of the RF excitation. On the other hand, studying the plasma behavior during the transition time is of considerable importance in order to understand the discharge ignition process. Moreover, pulsed discharges, which are important for several applications, such as the deposition of polymeric thin films [10], are strongly influenced by the transition time between the rise of the excitation signal and the reaching of the plasma steady state.

In this work, a review is presented concerning the information available in the literature about the temporal evolution of plasma parameters in RF-CCP discharges, with a special focus on the early stages after the discharge ignition or at the beginning of the turn-on phase in a pulsed discharge. A preliminary selection of papers for the literature review has been obtained using the Scopus and Web of Science databases, searching for papers that include in the title, abstract, or keyword sections the following terms: *plasma*, *ccp* or *capacitively-coupled*, *time-variation* or *time-evolution* or *evolution in time* or *ignition*. A surprisingly low number of publications was found, as low as 72 in the case of the Scopus database and 54 for Web of Science, with publication dates ranging from 1989 to 2023. The publications were then carefully selected on the basis of their abstract content, considering only the ones that described experimental research concerning the time evolution of plasma parameters during low-pressure RF-CCP discharges. Moreover, the bibliographic section of each paper was examined to search for other works of interest. Conference papers were not included in the review.

The review includes experimental works concerning the time evolution of plasma parameters in RF-CCP discharges, thus focusing on the publications that include measurements of the time evolution of some physical quantities involved in the plasma. However, several works also include simulation results or analytical models about discharge behavior.

The review has been divided into six sections: in the first one a very brief review about the main properties of RF-CCP discharges is provided; the second one reports about the reactor that was used as a reference in several of the publications reviewed; the third one deals with the time evolution of plasma parameters in continuous discharges; the fourth one covers the topic of pulsed discharges; the fifth one deals with the effects of parasitic discharges on the time evolution of plasma parameters; and the last one is devoted to some other topics, including the effect of powder formation and of the change of gas mixture composition during the discharge process.

2. Fundamental Properties of Low-Pressure RF-CCP Discharges

An example of a near-complete introduction to the properties of CCP plasma discharges can be found in the recent review paper by Chabert et al. [8], while in this section, only a very brief summary of the main discharge properties will be given. Capacitively coupled radio frequency discharges rely on the application of a time-varying electric field to a gas mixture by means of two electrodes, between which the gases are injected at a pressure lower than the atmospheric one. The simpler configuration involves the use of two planar parallel electrodes, one of which is usually grounded, while the other one is connected to a radiofrequency generator (usually working at 13.56 MHz) through a matching network, which is necessary to tune the load impedance in order to minimize the amount of power reflected to the generator. The time-dependent electric potential between the electrodes provides the energy required to accelerate the electrons inside the discharge, giving rise to the processes of ionization, excitation, and dissociation (if molecular gases are used) inside the gas mixture.

The space between the electrodes can usually be divided into three main regions: the plasma volume in the middle of the discharge, where the condition of quasi-neutrality is achieved and in which the electric potential is more positive than at the electrodes, and the two sheaths near the electrodes, where a depletion of negative charges is usually present, providing a stronger electric field that tends to accelerate ions towards the electrodes and to confine the electrons in the plasma bulk. The thicknesses of the two sheaths are characterized by an oscillating behavior, in which at different phases of the RF period,

one of the sheaths is suppressed, while the other one reaches its maximum extension, as discussed in Section 3.

The huge mass difference between electrons and ions causes different behaviors for the two particle types, producing a process of charge separation, which leads to the development of a DC component of the electric potential, usually called self-bias. The DC potential is more positive in the plasma bulk and drops in the two sheath regions towards the electrodes, thus accelerating the ions in the sheaths towards them. If the two electrodes have different areas, the potential drop is stronger towards the smaller electrode, which is usually the powered one, giving rise to an asymmetric RF-CCP discharge. These kinds of discharges are often used when a strong ion acceleration is desired toward only one of the electrodes, such as in sputtering deposition processes or in reactive ion etching.

Inside of the plasma bulk, different kinds of electron energy distribution functions (EEDF) can be achieved depending on the plasma conditions: a Maxwellian-like distribution is more frequent when molecular gases are uses, while a Druyvesteyn-like one is more common for atomic gases. The mean electron energy in the bulk region of RF-CCP discharges is usually of the order of a few electron volts, but the tails of the EEDF extend to more than 10 eV, providing electrons with sufficient energy to activate the ionization processes. The transfer of energy between the electron and ions is very inefficient due to the huge mass energy, and ions receive lower acceleration from the electric field due to their much greater inertia, so the mean ion energy in the plasma bulk is several orders of magnitude lower compared to electrons.

Secondary electrons can be emitted from the electrodes as a result of the interaction between the ions and the electrode surfaces and can be strongly accelerated towards the plasma bulk by the sheath electric field, reaching high energies and contributing to the ionization of the gas atoms and molecules. When these kinds of ionization processes are dominant, the discharge is said to work in the γ mode, while if the ionization happens mainly in the plasma bulk, the α mode is achieved. Other operation modes are also possible, as described in Section 3.

Besides continuous discharges, in which the RF potential is continuously applied between the electrodes, pulsed discharges are also possible, in which times of RF activation are alternated with times in which the bias is suppressed. These kinds of discharges, which are discussed in Section 4 of this review, have become more common in recent years due to their ability to provide a better control of some plasma parameters in etching processes.

3. The GEC Reference Plasma Reactor

A fundamental paper was published in 1991 by Hargis and a large collective of researchers from several research laboratories [11]. While this work does not provide any result concerning the time evolution of plasma quantities in a discharge, it was included in this review since it is often cited in subsequent publications as a reference for the experimental and theoretical analysis of CCP plasma discharges. In the paper, a standard reference cell was defined, named the *gaseous electronics conference radio frequency reference cell*, or *GEC cell* in its abbreviated form. This kind of cell consisted of a cylindrical stainless-steel chamber equipped with two round parallel electrodes, each having a diameter of 102 mm and positioned at a distance of 25.4 mm from the other. The electrodes were isolated from the chamber walls in order to allow them to be biased or ground independently or to leave them to float. The gas mixture was injected from the top electrode, using a showerhead configuration, while the exhaust gases were pumped away from four pumping ports located in the lateral walls, as shown in Figure 1. Such an unusual pumping configuration was used to reduce azimuthal variations in the gas pumping speed in order to minimize variations in the concentration of chemical species.

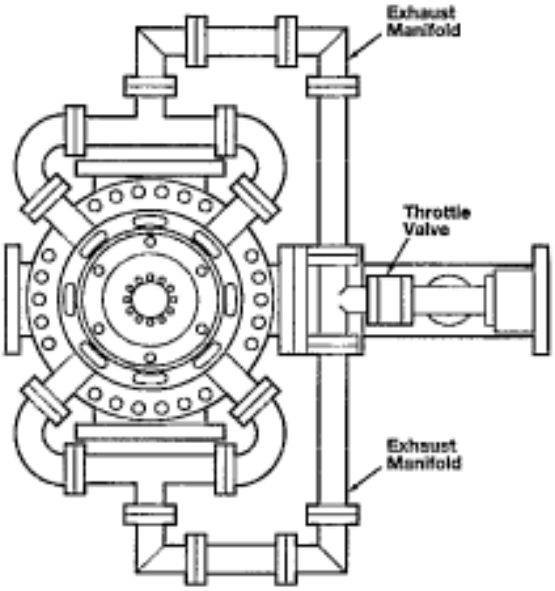

Figure 1. Schematic diagram of the GEC reference cell pumping apparatus. The four pumping windows are visible in the diagram. Reprinted from [11], with permission of AIP Publishing.

An experimental analysis of the electrical characteristics was carried out for plasma discharges activated using Ar gas in GEC reference cells with an identical design produced by different manufacturers in order to test the reproducibility of plasma conditions. To this aim, a set of sinusoidal excitation signals, with specific peak-to-peak voltage values, were applied to the cells at different values of Ar pressure and a fixed gas flow rate of 20 sccm. The voltage and current signals in the discharge were then measured, and a Fourier analysis of the measured voltage and current waveforms was carried out, considering the first five Fourier components. A simplified electrical circuit, shown in Figure 2, was used to describe the electrical behavior of the cells.

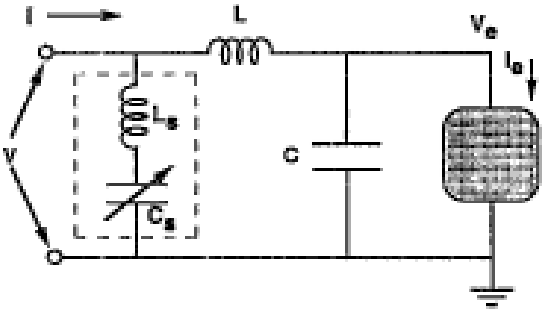

Figure 2. A simplified electrical circuit used to describe the GEC cell behavior. V is the voltage signal applied to the cell, upstream of the matching network, while V_e and I_e are the voltage and current measured between the electrodes. L, L_e, and C_s are the inductors and the capacitor included in the matching network. Reprinted from [11], with permission of AIP Publishing.

The results of the electrical characterization of the cells are shown in Figure 3, where the current passing between the electrodes is shown as a function of the voltage difference between them. In the picture, the data measured on different GEC cells in different laboratories are reported together, with a line representing a least square linear fit of the data and two lines representing the one standard deviation of the data from the fitted line. According to the results, a good agreement between the electric measurements performed on the different cells is evident.

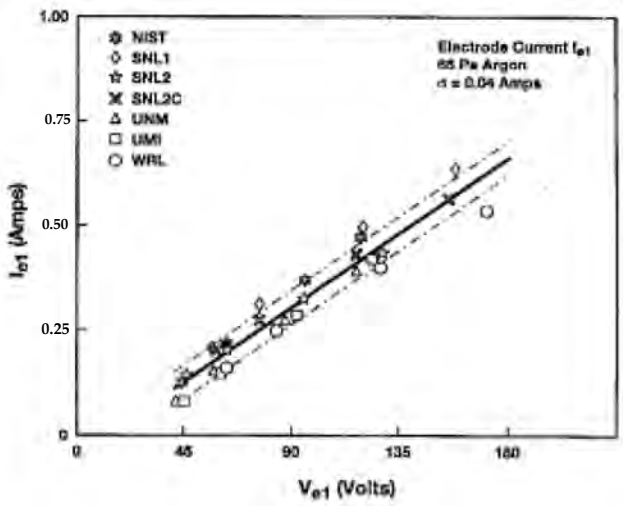

Figure 3. Dependence of the electrode current on the electrode voltage in GEC reference cells manufactured in different laboratories. The solid line is a linear fit to the data, while the dot-dash line represents the one-sigma standard deviation from the fitted line. Reprinted from [11], with permission of AIP Publishing.

4. Time Evolution of Plasma Parameters during RF Cycles of Continuous Discharges

4.1. Time Evolution of the Plasma Potential and Electron Temperature in Ar Discharges

The earlier experimental work found in the research results, which was published by Wilson and coworkers in 1989, ref. [12] included a temporal analysis of the plasma potential, as well as the electron temperature and density in an RF-CCP discharge activated in a commercial plasma etcher in Ar gas at a pressure of 53.3 Pa, a power of 100 W, and a peak-to-peak RF amplitude of 72 V. The time-varying floating potential, measured by means of a capacitive probe, was found to be of sinusoidal shape, with an amplitude of (42.1 ± 1.6) V and a DC reference, measured using a high-input impedance Langmuir probe, of (-4 ± 0.7) V. The plasma potential, obtained from the I-V characteristic curve, was found to vary between (51.0 ± 1.6) V and (9.0 ± 1.6) V. The time-varying current was measured by a low-input impedance Langmuir probe and the shape of the resulting I-V characteristic curve, measured at the time of maximum and minimum bias voltage, is shown in Figure 4. The plot shows the average and instantaneous current as a function of the bias voltage, with the instantaneous current measured at the times at which the plasma potential assumed its minimum and maximum values, respectively.

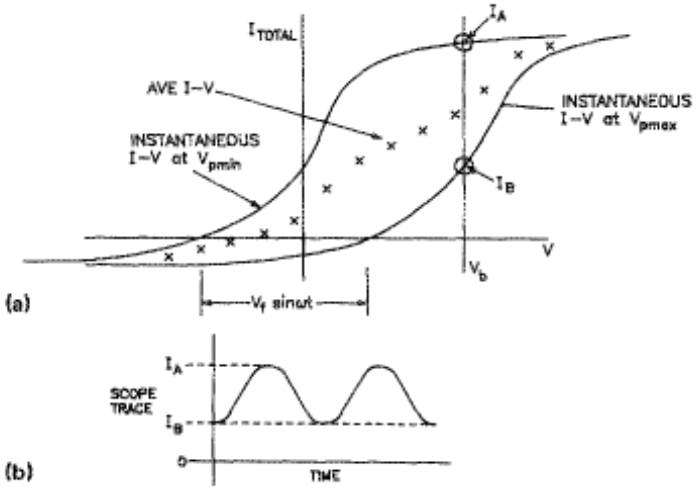

Figure 4. Plot representing the average (crosses) and instantaneous (continuous lines) current as a function of voltage (**a**). The instantaneous current is measured at the time of minimum (V_{pmin}) and

maximum (V_{pmax}) bias voltage. Plot of the typical scope trace of instantaneous current (**b**), where I_A occurs at V_{pmin} and I_B occurs at V_{pmax} for an applied bias voltage V_b. Reprinted with permission from [12]. Copyright 1989, American Vacuum Society.

4.2. Sheaths Motion in Ar, He, and H_2 Discharges

In another interesting study published by Wood and coworkers in 1991, ref. [13] the motion of the sheaths during an RF-CCP discharge in Ar was investigated through experimental and theoretical means. A circuit model was developed for the physical system composed of the discharge and a Langmuir probe, in order to relate the voltage measured by the probe to the sheath motion. The model equation was solved numerically, obtaining waveforms that were comparable with the observed ones. Unfortunately, the digitalized version of the paper shows very degraded images, so the comparison between experimental data and calculated curves is quite difficult.

The time-resolved dynamics of sheaths in an RF-CCP discharge was investigated by Czarnetzki and coworkers [14] in 1998. The authors used a *laser-induced fluorescence* technique (LIF) to measure the time-resolved voltage in the sheaths of asymmetric He and H_2 GEC reference discharges by exploiting the Stark effect. The measured time evolution of the sheath voltage at the powered and ground electrodes in the He discharge is shown in Figure 5. The voltage was obtained by integrating the electric field measured by the LIF technique. The authors also compared the measured quantities with a model description of the ion and electron motion in the discharge and found a reasonable agreement. The sheath voltage measured at the ground electrode in the H_2 discharge as a function of time is shown in the lower graph of Figure 6, while the upper section of the figure shows the time- and space-resolved excitation rate for the excitation of hydrogen atoms to the state with $n = 3$. It is worth noting that the peak of sheath voltage between 25 and 45 ns (evidenced by the red lines in Figure 6) corresponds to a region of high excitation near the electrode, while another region of high excitation appears between 45 and 55 ns, when the sheath voltage has been already suppressed. The authors provide quite elaborated explanation of this behavior, which cannot be reported in this review due to space limitations.

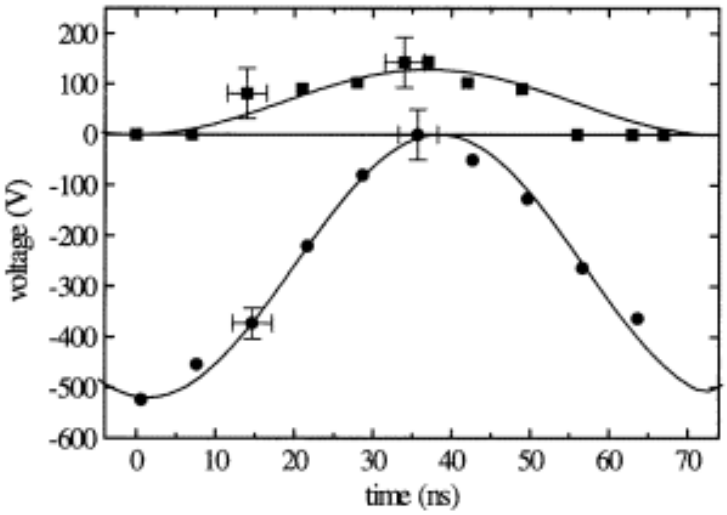

Figure 5. Time evolution of the voltage measured over the sheaths at the grounded (■) and powered (●) electrodes in a GEC He discharge at a pressure of 50 Pa, a gas flow rate of 90 sccm, and a peak-to-peak bias voltage of 700 V. The solid lines are sinusoidal fits. © IOP Publishing. Reproduced with permission from [14]. All rights reserved.

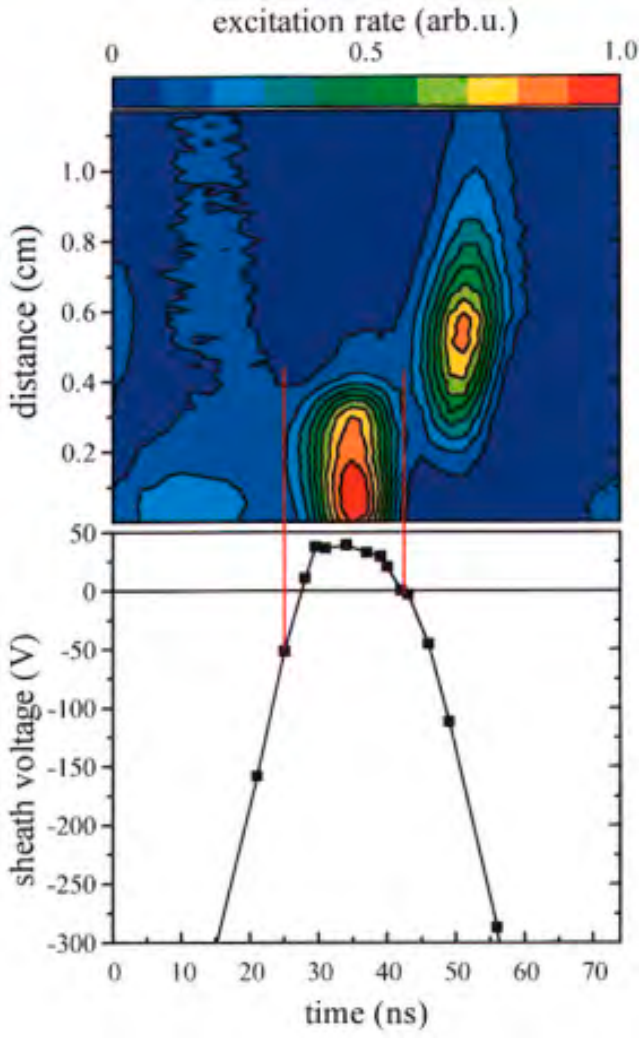

Figure 6. Time and space resolved excitation rate to the n = 3 state of atomic hydrogen (**upper graph**) and time evolution of the sheath voltage at the powered electrode (**lower graph**) in a GEC H_2 discharge at a pressure of 80 Pa, a gas flow rate of 90 sccm, and a peak-to-peak bias voltage of 650 V. © IOP Publishing. Reproduced with permission from [14]. All rights reserved.

In 2020, an important effect was discovered by Sun and coworkers in a simulation study ref. [15] that is related to the effect of strong electron emission from the electrodes of a CCP discharge on the behavior of the sheaths and the plasma volume. The resulting discharge, which was called *inverted RF plasma* (IRF) by the authors, is characterized by a linear potential drop in the central region of the discharge, while two small sheaths are located near the electrodes, in which the electric field direction is inverted compared to a normal RF-CCP discharge. The potential drop in the central region is much greater compared to the ones located in the inverted sheaths. The authors did not include any experimental data in their work, which is purely based on 1D1V kinetic simulations, but it was included in this review due to its importance.

4.3. Time Evolution of Rotational Temperature in H_2 Discharges

The time evolution of the rotational temperature of H_2 molecules in a GEC discharge was reported in a study published by Gans and coworkers in 2001. Ref. [16] The authors used a high resolution camera to measure the intensity of emission peaks in a specific range of the Fulcher-α band of the H_2 spectrum. Two peaks of the emission intensity were observed during each RF cycle, at different times near the end of the cycle, and different distances from the powered electrode. The farthest peak from the powered electrode was

attributed to the emission of electrons from the space charge region into the plasma region. On the other hand, the peak closer to the electrode was considered due to the acceleration of electrons emitted from the sheath towards the electrode during the electric field reversal at the end of an RF cycle. A mathematical model was developed by the authors to explain the behavior of the rotational temperature with time within an RF cycle, and a comparison between the model and the experimental results is shown in Figure 7.

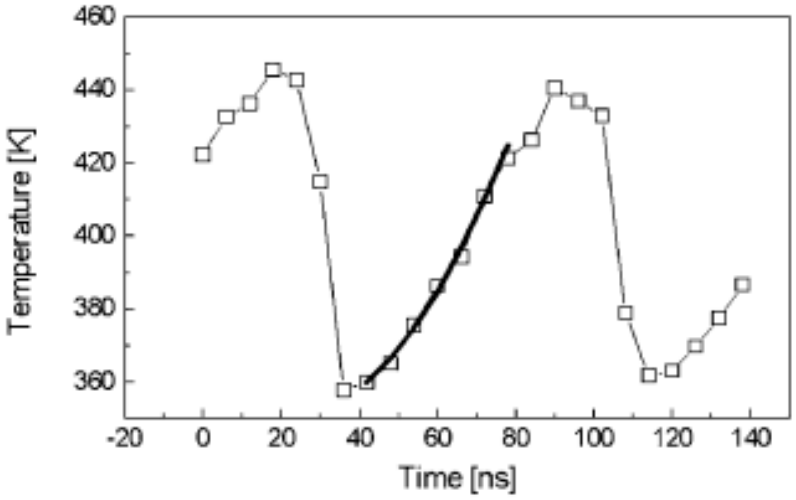

Figure 7. Time evolution of the rotational temperature of hydrogen molecules in a GEC H_2 discharge at a pressure of 42 Pa, gas flow rate of 50 sccm, and an RF power of 100 W. The thick solid line represents the result from a mathematical model. © IOP Publishing. Reproduced with permission from [16]. All rights reserved.

4.4. Transition between α Mode and Drift-Ambipolar Mode in CF_4 Discharges

Capacitively coupled discharges may work in two main different operation modes, usually named *α mode* and *γ mode*; in the former, the ionization processes are mainly activated by the electrons in the bulk of the discharge, while in the latter, they are mainly produced by the secondary electrons accelerated inside the sheaths. Ref. [8] However, other operation modes may exist, and a specific one, named *drift-ambipolar mode* (DA mode), was identified in a study published in 2011 by Shulze and coworkers, ref. [17] for the specific situation of the strongly electronegative CF_4 gas. The authors exploited a combination of experimental analyses, including *phase-resolved optical emission spectroscopy* (PROES), computer simulations, by means of the *particle in cell* with Montecarlo collision method (PIC-MCC), and an analytical model. The authors identified two main components in the electric field inside of the discharge during the DA mode: a nearly uniform drift field, mainly due to the low DC conductivity in the bulk of the discharge, and an ambipolar one, peaked near the sheath edge and mainly due to the accumulation of electrons in that region. Figure 8 shows the simulation and experimental results obtained by the authors in two CF_4 discharges working at a pressure of 40 Pa and peak bias voltages of 100 V and 400 V, respectively. The DA mode can be observed at the lower voltage (left column of images) where the peak of the calculated ionization rate and the corresponding measured light emission peak is observable near the two sheaths edges during one RF period. On the other hand, at a peak bias voltage of 400 V the α mode is observed, in which the ionization rate peak moves in the bulk region between the two sheaths. Figure 9 shows a similar transition, while keeping constant the peak bias voltage at 200 V and changing the total pressure from 40 to 80 Pa. At the lower pressure a hybrid situation between the α and the DA mode is observed, while increasing the pressure a pure DA mode is achieved.

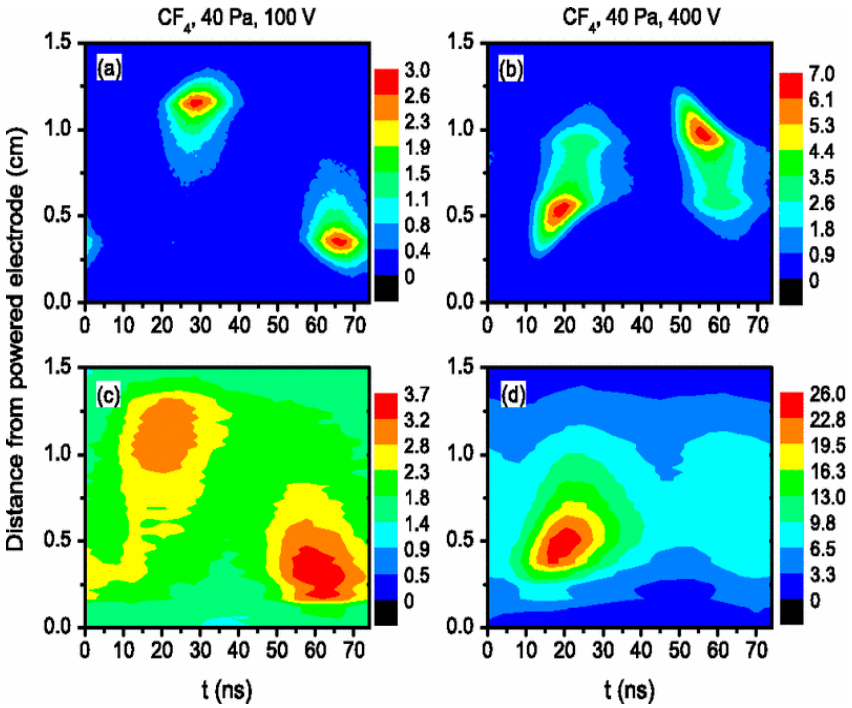

Figure 8. Plasma parameters as a function of time and space in a CF_4 discharge working at 40 Pa. In the first row, ionization rates from PIC-MCC simulations are reported in unit of 10^{21} m^{-3} s^{-1} for 100 V (**a**) and 400 V (**b**) peak bias voltages, while in the bottom row the measured plasma emission at 250 nm is reported in arbitrary units for 100 V (**c**) and 400 V (**d**) peak bias voltages. Reprinted with permission from [17]. Copyright (2011) by the American Physical Society.

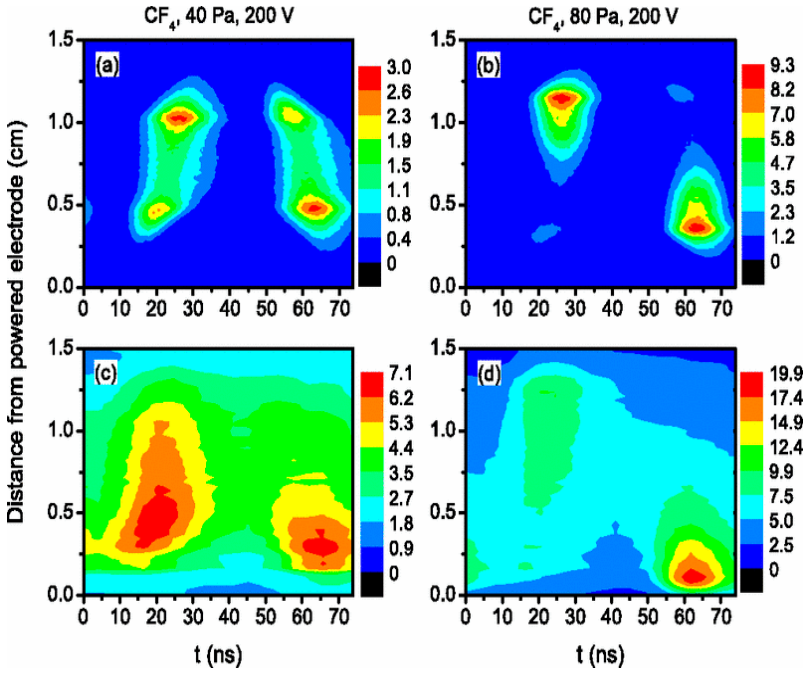

Figure 9. Plasma parameters as a function of time and space in a CF_4 discharge working at 200 V peak bias voltage. In the first row, ionization rates from PIC-MCC simulations are reported in units of 10^{21} m^{-3} s^{-1} for pressure of 40 Pa (**a**) and 80 Pa (**b**), while in the bottom row the measured plasma emission at 250 nm is reported in arbitrary units for pressure of 40 Pa (**c**) and 80 Pa (**d**). Reprinted with permission from [17]. Copyright (2011) by the American Physical Society.

4.5. Effect of Electrode Non Planar Features on the Plasma Parameters in Ne Discharges

The effects of specific non-planar features on the surface of the powered electrode were presented in an interesting study published by Shmidt and coworkers in 2013 [18]. The authors measured the time-dependent behavior of the excitation rate in a modified GEC cell working with pure Ne with an RF bias amplitude of 264 ± 4 V, using a 2D phase-resolved optical emission spectroscopy (PROES), and the results are shown in Figure 10. In the top row of the figure, a plot shows the time evolution of the applied RF voltage, while the images in the lower rows represent the excitation rate, as a color scale in arbitrary units, in the region near the structured electrode, measured over a duration of 5 ns at different times in the RF period. A remarkable amplification of the excitation rate is visible near the trenches as compared with the situation of the planar electrode, especially for triangular-shaped structures. According to the authors' interpretation, the excitation intensity follows the expansion in time of the plasma sheaths, and a strong amplification is achieved when electrons accelerated by sheaths moving in convergent directions meet in a certain region, as in the case of the triangular trenches.

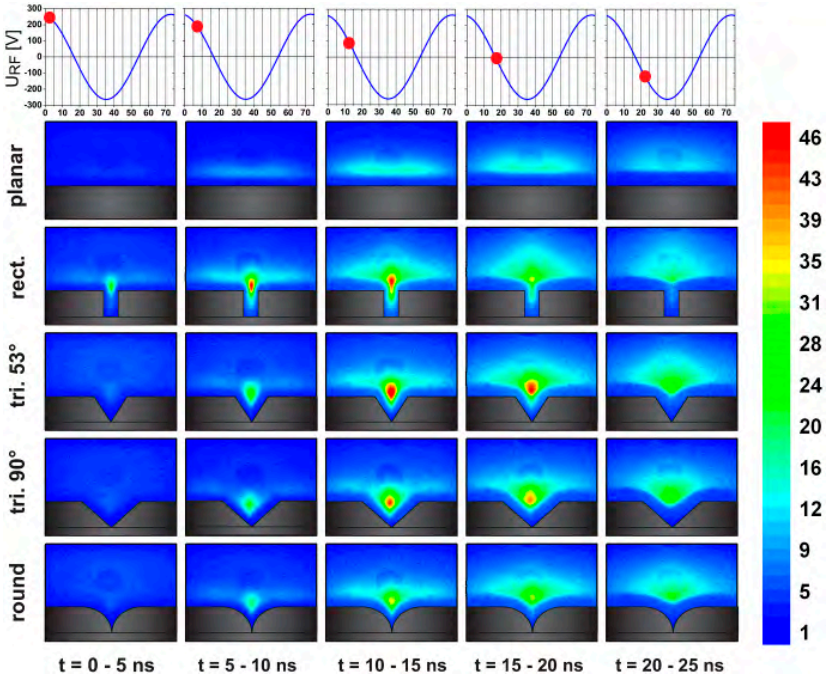

Figure 10. Time-resolved excitation rate near the structured powered electrode in a Ne discharge working at 10 Pa and 264 V peak RF amplitude, with electrode structures. The first row shows the time evolution of the RF bias on the electrode. © IOP Publishing. Reproduced with permission from [18]. All rights reserved.

4.6. Radial Dependence in the Time Evolution of Plasma Parameters in Ar Discharges

In 2021, the radial dependence of several plasma parameters as a function of time in Ar discharges was investigated experimentally by Su and coworkers. Ref. [19] Figure 11 shows the results of electron density in a semi-logarithmic scale, where the upper horizontal axis in the graphs reports the time elapsed from the pulse start and the lower horizontal axis shows the corresponding number of RF periods. According to the authors, the electron density was too low to be measured during the first 54 RF periods, then started to rise very rapidly for a few microseconds and, after about 63 RF periods, began to lower its rate of rise. This behavior is very similar at all the distances from the central axis up to about 15 cm, which is the electrode radius, while it changes to a lower increase rate at 16 cm, which correspond to a position outside the cylindrical volume between the electrodes. Figure 12 shows the light emission intensity at 750.4 nm as a function of time and radial position. As can be seen from the graph, the light emission is not measurable for the first

46 RF periods due to too low of an electron density and RF power absorbed in the plasma. Differently from the electron density, the light emission intensity shows a remarkably different time evolution at different radial positions, with a much greater initial overshoot near the center of the discharge volume, which is completely suppressed in the discharge periphery. According to the authors, the light emission overshot in the center region should be related to a similar behavior of the electron density, which is not observed. The authors attributed this inconsistency to a limitation of the procedure used in the measurement of the electron density using a hairpin probe due to the approximation applied to extract the electron density from the raw values, which considered a constant electron temperature.

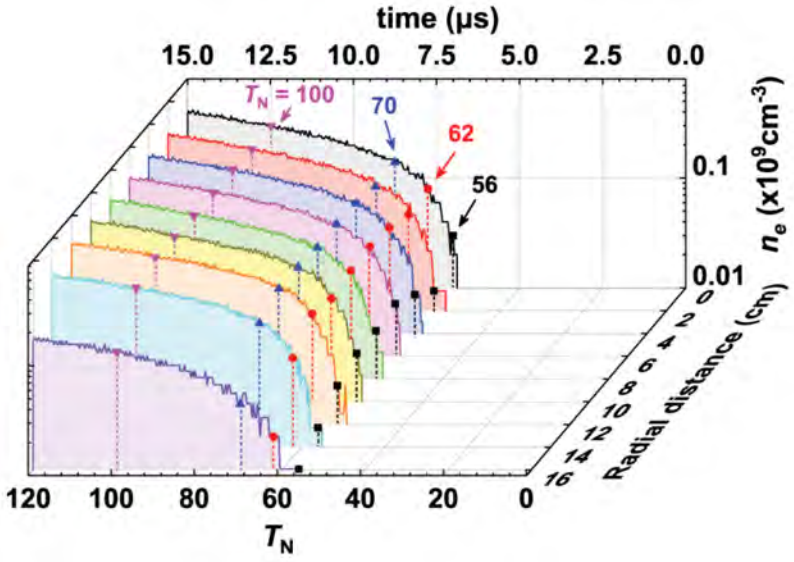

Figure 11. Time evolution of the electron density, shown in a semi-logarithmic scale at some radial positions during the first 120 RF cycles of an Ar RF-CCP discharge. The vertical lines in the graph show some specific RF cycles, T_N = 56, 62, 70, and 100. Reproduced from [19] by permission of IOP Publishing Ltd. All rights reserved.

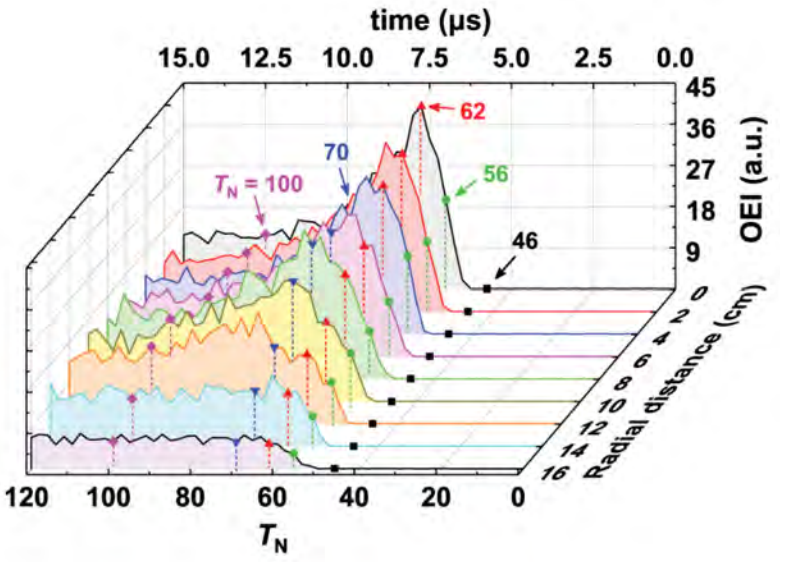

Figure 12. Time evolution of the optical emission intensity at 750.4 nm at some radial positions during the first 120 RF cycles of an Ar RF-CCP discharge. The vertical lines in the graph show some specific RF cycles, T_N = 56, 62, 70, and 100. Reproduced from [19] by permission of IOP Publishing Ltd. All rights reserved.

5. Time Evolution of Plasma Parameters in Pulsed Discharges

5.1. Overall Pulse Behavior in Pulsed Ar Discharges

An important work was published by Overzet and Leong-Rousey in 1995, ref. [20] in which experimental measurements of the main plasma electrical quantities were reported for a GEC reference cell working with Ar at a pressure of 500 mtorr and a 20 sccm flow rate, to which a pulsed bias was applied by means of a square wave signal with 500 Hz frequency. The voltage and current in the discharge, as well as the power absorbed, were measured as a function of time during the turn-on and turn-off phases of the pulse. The turn-on behaviors of voltage and current are shown in Figure 13a, where the electrical quantities are shown as a function of time in a semi-logarithmic plot: while the voltage follows the pulse shape, the current shows intense oscillations with a regular time interval of approximately 500 ns. A similar behavior was found during the turn-off phase of a pulse, as shown in Figure 13b, with the voltage that follows the pulse behavior and the current that oscillates with approximately the same frequency as in the turn-on phase. The authors measured the same quantities in the evacuated reactor and found oscillations of the current having the same period but a much lower amplitude. The time evolution of the power absorbed in the discharge during the turn-on of the pulse is shown in Figure 13c, where it is quite evident that the power rises with oscillations similar to the ones observed in the current. During the power-off of a pulse, instead, similar oscillations are still present, as shown in Figure 13d, but they are centered around the zero power value and show negative values, which are related to power being returned to the RF generator. A similar behavior was also measured in the emptied reactor without the plasma discharge. The authors attributed the presence of this reflected power to the energy stored in the resonant network between the probes and the electrodes, which was delivered to the generator during the power turn-off.

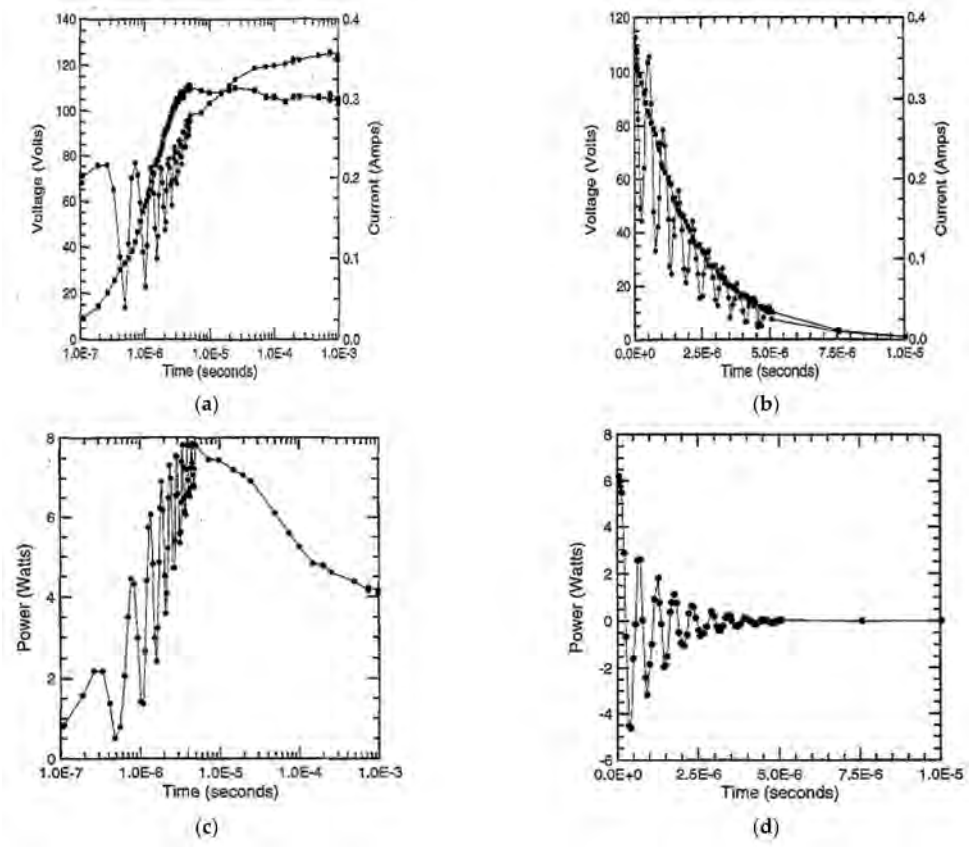

Figure 13. Electrical characterization of a CEG reference cell working with Ar at 500 mtorr and 20 sccm, powered by a pulsed RF signal (pulse frequency 500 Hz). Voltage between the electrodes (■)

and current flowing in the plasma (•) measured as a function of time during the turn-on (**a**) and turn-off (**b**) phases of a pulsed discharge. Power absorbed in the discharge as a function of time during the turn-on (**c**) and turn-off (**d**) phases of a pulse. © IOP Publishing. Reproduced with permission from [20]. All rights reserved.

The authors used a theoretical model to estimate the time evolution of the electron collision frequency during the turn-on phase of a pulse from the measured electrical quantities, as shown in Figure 14. According to their estimation, the collision frequency rises strongly in the first few microseconds after the RF power activation, reaching a value of approximately 2×10^{10} Hz, and then decreases by about one order of magnitude after one millisecond. This behavior was explained by the fact that at the very beginning of the pulse the sheaths are not yet formed, and most of the RF power is released in a discharge bulk, while as the sheaths start to be generated they absorb an increasingly high fraction of the power.

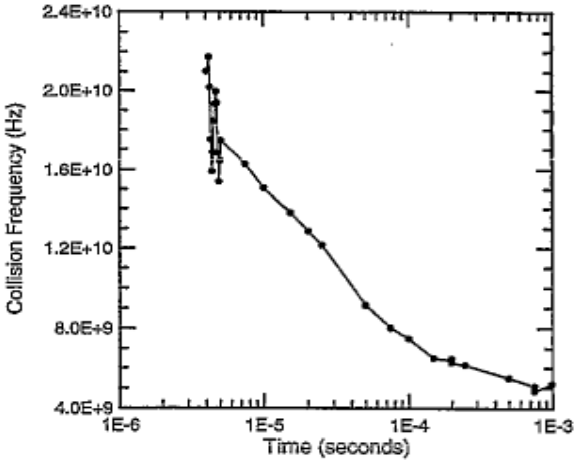

Figure 14. Estimated electron collision frequency as a function of time during the turn-on of a pulse in a CEG reference cell working with Ar at 500 mtorr and 20 sccm, powered by a pulsed RF signal (pulse frequency 500 Hz). © IOP Publishing. Reproduced with permission from [20]. All rights reserved.

5.2. Overall Pulse Behavior in Pulsed Discharges Using Ar + He Mixtures

Another paper dealing with the study of pulsed discharges in a GEC cell was published in 1998 by Overzet and Kleber. Ref. [21] In this study, discharges based on He, Ar, and a He + Ar mixture were investigated using a Langmuir probe (LP) and a microwave interferometer (MWI). The RF power signal was modulated by a square wave with a period of 50 ms or 2 ms, a duty cycle of 50%, and a modulation of 100%. A quite complete characterization of the plasma discharge was carried out by the authors, including a measurement of the plasma potential, floating potential, electron density, ion density, and electron effective temperature (kT_e). Figure 15 shows the normalized electron density (n_e) measured in He and Ar discharges working at 300 and 100 mtorr, respectively, pulsed by a square wave of 50 ms period and measured by means of MWI during a cycle of the pulse wave. The two quantities were normalized to assume the same value in the graph during the active phase of the pulse, which corresponds to the region before t = 25 ms in the graph. At the pulse turn-on, as shown at the left end of the graph, the time required for the electron density to reach a steady-state is much shorter in the He discharge (shown as circles in Figure 15) than in Ar (shown as a continuous line in Figure 15). At the pulse turn-off, at t = 25 ms, the electron density strongly rises in the He discharge, before being reduced to a negligible value. On the other hand, in Ar, a more complex behavior is visible in the time evolution of the electron density after turn-off, with a reduction, followed by a rise, and then by a subsequent reduction.

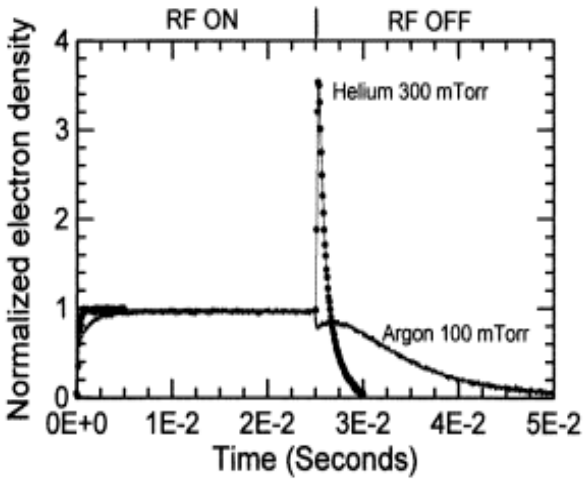

Figure 15. Normalized electron density measured by means of MWI in He (circles) and Ar (continuous line) discharges working at 300 and 100 mtorr, respectively, measured by means of MWI during a pulse of 50 ms total duration (turn-on plus turn-off phase). © IOP Publishing. Reproduced with permission from [21]. All rights reserved.

The increase of electron density after the discharge extinction is explained by the authors considering the presence in the He and Ar discharges of atoms in metastable excited states, which can give rise to an additional form of ionization when the electron energy has become negligible after the discharge turn-off. To justify this explanation, the authors have considered a comparison between the electron densities obtained by MWI and by the Langmuir probe in the He discharge, as shown in Figure 16, which is related to a pulse period of 2 ms. In fact, considering the He discharge behavior shown in Figure 16a, a rise in the electron density after the pulse shut-off at t = 1 ms is observed by both the MWI and the Langmuir probe analyses, while, during the same time, the electron temperature has already reached negligible values. An ionization mechanism different from electron-impact must be considered to explain this rise in electron density, which could be given by the presence of He metastable excited atoms. In order to confirm this explanation, the authors also measured electron energy distribution function after the pulse shut-off and found a peak at an energy value which is compatible with the emission of electrons from He metastable excited states.

A different behavior was measured in an Ar discharge, as shown in Figure 16b, where a totally different time evolution is seen after the pulse turn-off for the electron density measured by MWI and the Langmuir probe, with the former slowly rising and the latter decreasing abruptly. Moreover, the electron temperature reduction after the pulse turn-off requires about 100 μs in He, as seen in Figure 16a, and a much shorter time required in Ar, as shown in Figure 16b. The authors noted that the values shown in Ar after this time are not reliable, as evidenced in the graph. The larger time required to reduce electron temperature in He was addressed by the authors to the larger mass of the Ar atoms compared to the He ones, which involved a lower efficiency of energy transfer from electrons to atoms during elastic collisions after the plasma turn-off. In order to explain the difference between the electron density measured by MWI and the Langmuir probe, the authors considered that the former technique provides an average value of the plasma parameter mediated over all the reactor volume, including the part not involved in the plasma discharge. On the other hand, the Langmuir probe provides a measure related to a relatively small volume, located in the space between the electrodes. According to the authors' interpretation, the slower electron temperature decrease in He plasma produces a slower decrease in the electron loss rate, which compensates for the ionization provided by the metastable excited atoms presence in the region between the electrodes.

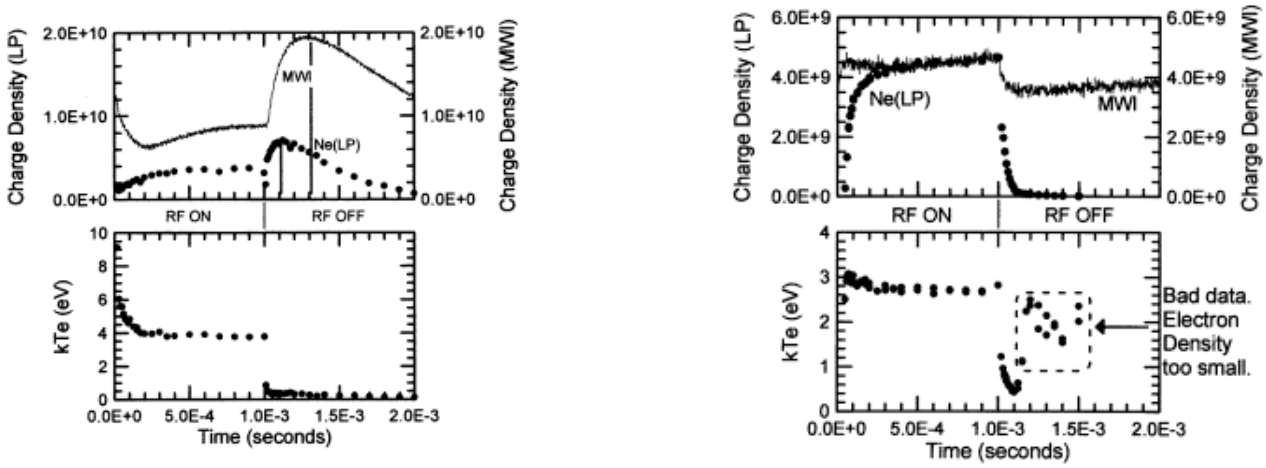

(**a**) (**b**)

Figure 16. Electron density (shown as circles in the upper graph) and electron temperature (shown as circles in the lower graphs) measured by a Langmuir probe, and electron density measured by MWI (shown as continuous lines in the upper graphs) as a function of time. The values are measured in a He discharge at 500 mTorr, 30 sccm and 200 V RF amplitude (**a**), and an Ar discharge at 100 mTorr, 20 sccm and 200 V RF amplitude (**b**), during a pulse of 2 ms total duration (turn-on plus turn-off phase). © IOP Publishing. Reproduced with permission from [21]. All rights reserved.

5.3. Afterglow Region in Pulsed Ar Discharges

In 2010, an interesting work from Samara and coworkers was published, ref. [22] which included an experimental analysis of the electron density and the light emission behavior in the afterglow region of a pulsed Ar GEC discharge. The electron density was measured by means of Langmuir and hairpin probes, while the light emission was investigated by means of a spectrometer and a CCD camera. The authors investigated Ar discharges working at pressure values in a range from 7 to 70 Pa and RF power ranging between 2 and 100 W, which were pulsed by means of different kinds of signals.

A simpler situation is shown in Figure 17, where the time-dependent behavior of light emission and electron density is shown for a discharge working at 27 Pa and 50 W, pulsed through a rectangular wave with a period of 1 ms and a duty cycle of 50%. The light emission signal was obtained by integrating the radiation emitted from the discharge in the range of wavelengths between 300 and 900 nm and normalizing it to the value measured in the non-pulsed discharge. This parameter was used by the authors to evaluate the electron temperature since the two quantities are strictly related and the latter shows much greater instability during the discharge. The optical emission shows an abrupt peak at the beginning of the pulse, followed by reduction and stabilization, and drops quickly after the pulse turn-off. On the other hand, the electron density increases more smoothly after the pulse turn-on, reaching a stable value after about 250 μs, and drops following a two-step linear behavior after the RF turn-off. Moreover, it shows a short pulse immediately after the RF turn-off, which may seem to be a surprising behavior since the electron energy is quickly decreasing in that part of the pulse. The authors provide an explanation for this behavior, considering that when the electric field vanishes, the electrons cool rapidly due to elastic collisions with the gas atoms, thus reducing their speed and increasing the time they remain in the region between the electrodes. Moreover, new electrons can be produced even when the electron temperature has already vanished, thanks to the Penning ionization process.

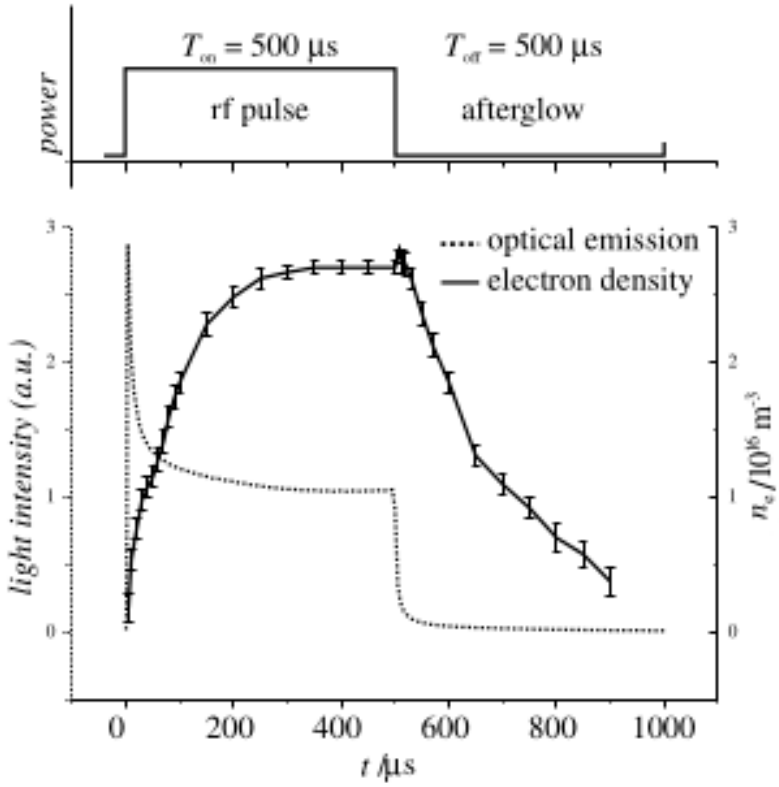

Figure 17. Light emission intensity (dashed line, scale on the left) and electron density (continuous line, scale on the right) measured in a pulsed GEC cell working at 27 Pa and 50 W in Ar. The light emission intensity is normalized to a non-pulsed discharge. © IOP Publishing. Reproduced with permission from [22]. All rights reserved.

More complex situations are shown in Figures 18 and 19, where the time evolution of electron density and light emission intensity are shown for two different types of pulse as continuous lines, while the same evolution for the rectangular pulse is also reported as a dashed line for comparison. In Figure 18, a linear increase in the RF amplitude is applied in the turn on phase of the pulse, followed by an abrupt turn-off. On the other hand, in Figure 19, the opposite behavior is considered, in which an abrupt turn-on is applied, followed by a linear decrease in amplitude in the turn-off phase. Compared with the situation of a square wave modulation, the situation in Figure 18 shows the absence of an overshoot of the light emission, and therefore of the electron temperature, at the RF turn on. Moreover, the electron density rises more slowly while reaching a very similar final value. The turn-off phase, on the other hand, is very similar for the rectangular wave and the modified one.

The situation shown in Figure 19 is very different from the case of the rectangular wave, both at the turn-on and turn-off phases of the pulse signal. In fact, at the pulse beginning there is an overshot of the light emission for both the rectangular and the modified pulse waves but it is followed by a signal stabilization at different values, with the higher one being observed for the modified wave. The authors suggested that this difference could be due to the presence of different electron energy distributions in the afterglow region in the two situations. In the turn-off region, the optical emission shows a less abrupt decrease with the modified wave, while the electron temperature shows an anticipated decrease and does not show the short pulse that is present with the rectangular wave pulse. These results are interesting in the view of a better control of the plasma properties during pulsed discharges.

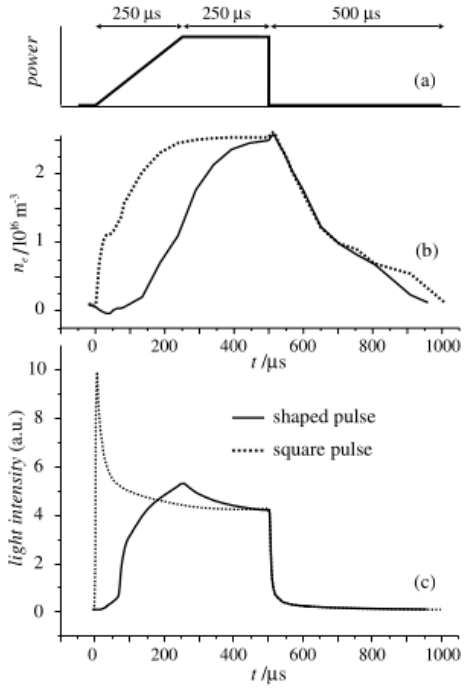

Figure 18. Electron density (**b**) and light emission intensity (**c**) in an GEC cell working at 27 Pa and 50 W in Ar and pulsed with a rectangular signal (dashed lines) and a signal shaped as shown in (**a**) (continuous line). The light emission intensity is normalized to a non-pulsed discharge. © IOP Publishing. Reproduced with permission from [22]. All rights reserved.

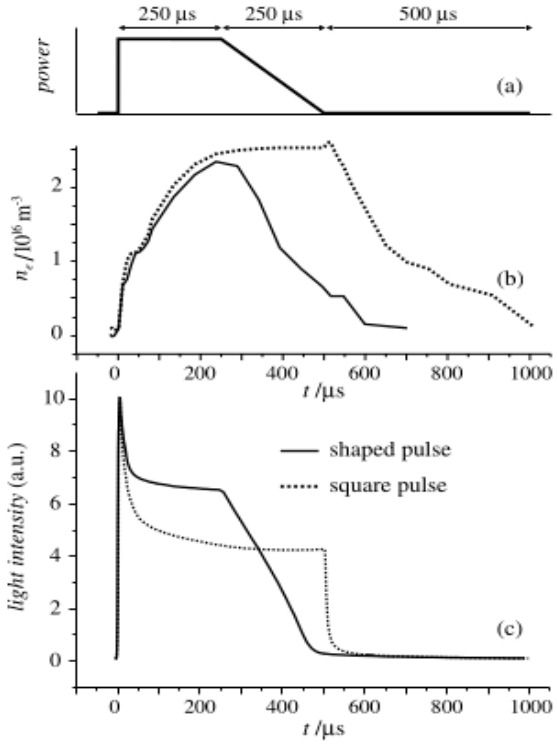

Figure 19. Electron density (**b**) and light emission intensity (**c**) an Ar GEC cell working at 27 Pa and 50 W and pulsed with a rectangular signal (dashed lines) and a signal shaped as shown in (**a**) (continuous line). The light emission intensity is normalized to a non-pulsed discharge. © IOP Publishing. Reproduced with permission from [22]. All rights reserved.

5.4. Re-Ignition Phase in Pulsed Ar Discharges

The phases of plasma turn-off and re-ignition are of paramount importance in pulsed discharges, and the physical mechanisms involved have been the subject of considerable interest in the scientific community. In recent years, an interesting study about this topic was published by Lee and coworkers, ref. [23] in which the plasma ignition during the turn-on phase of Ar pulsed discharges was investigated by means of plasma emission spectroscopy. The results of the total optical emission, measured as a function of time during the ignition phase of a pulse are show in Figure 20, where, in each of the plots, one of the parameters among applied power, pressure, and distance between the electrodes was varied, while keeping fixed the other two. Figure 20a, in which only the power is changed, shows how this parameter determines the final optical emission intensity, after the ignition phase, while in the other two plots, where the power is fixed, the final intensity does not change. The variation of pressure, as can be seen in Figure 20b, shows how this parameter has a strong influence on the time required to reach a stable emission level after the pulse turn-on, showing an increase in the time lag when the pressure is reduced. The authors suggest that this behavior is mainly related with the reduction induced in the electron density when the pressure is lowered, which causes a reduction in the electron collision rate, thus increasing the time lag. Figure 20c shows how the time lag is reduced with a reduction in the electrode distance, which can be related to the consequent increase in the electric field intensity.

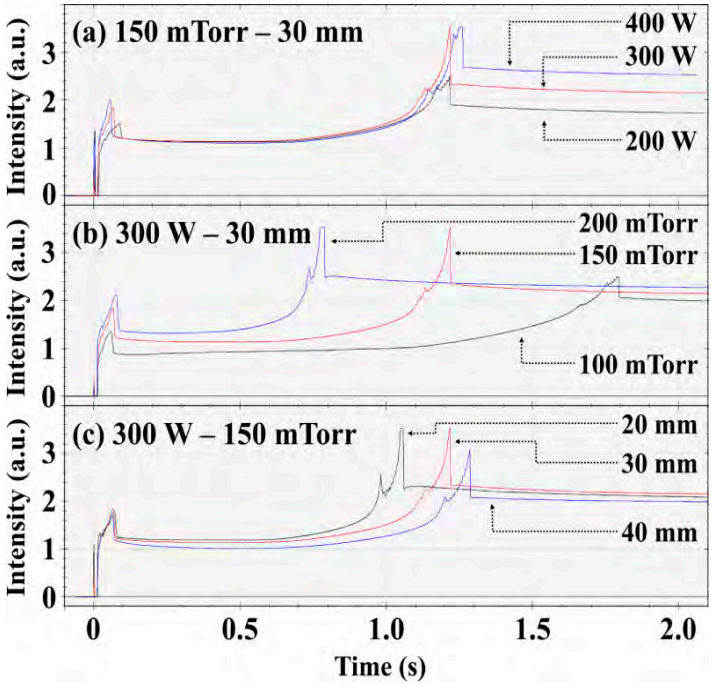

Figure 20. Total light emission forms a pulsed RF (13.56 MHz) CCP discharge in Ar during the ignition step of a pulse. In the different plots the results are show for the variation of a different parameter: (**a**) fixed pressure and inter-electrode distance, while varying the applied power; (**b**) fixed power and inter-electrode distance, while varying the pressure; (**c**) fixed pressure and power, while varying the inter-electrode distance. © The Japan Society of Applied Physics. Reproduced from [23] by permission of IOP Publishing Ltd. All rights reserved.

Another interesting work related to pulsed discharges was published in 2020 by Hernandez and coworkers [24], in which the authors investigated the electron heating mechanism in a pulsed RF (13.33 MHz) CCP discharge in Ar by means of *phase-resolved optical emission spectroscopy* (PROES). The discharge was pulsed by means of square waves with frequencies of 0.1 kHz and 10 kHz and a 50% duty cycle, and the results observed with

the two frequencies were compared, while the emission intensity was filtered to isolate the 750.4 nm emission line. The authors especially investigated the phenomenon of plasma emission and electron temperature overshoot that is observed during the re-ignition of a plasma discharge in the turn-on phase of a pulsed discharge.

In Figure 21, the excitation rate of Ar is reported as a function of time and space for a discharge pulsed with a wave of 10 kHz frequency. Each plot of the figure shows a time window of 150 ns duration, corresponding to two RF periods, starting at different discharge times, as follows: Figure 21a shows the first RF period in which the optical emission was strong enough to allow the extraction of the excitation intensity from the optical emission data; Figure 21b shows the RF period in which the overshoot takes place; Figure 21c shows the first RF period in which the plasma reaches the steady state; and Figure 21d shows an RF period at a time when the steady state was completely established. In all four graphs in this figure, the excitation rate assumes a peak value once per period, during the time of the period in which the sheaths are expanding from the electrodes towards the center of the discharge and are moving away from the powered electrode. Moreover, a single excitation peak is observed for each RF period in all four time windows investigated. According to the authors, this behavior is consistent with an α mode of electron heating.

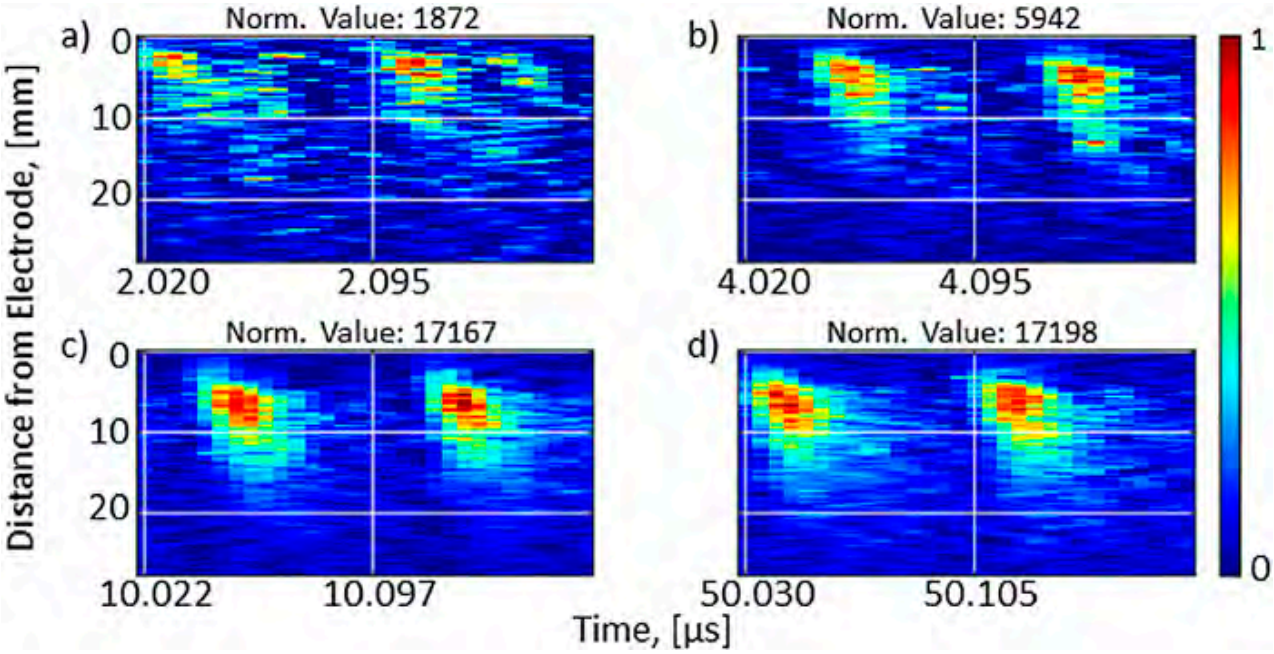

Figure 21. Excitation rate, measured at different times and distances from the powered electrode (at 0 mm) during the re-ignition of an Ar CCP discharge pulsed by a 10 kHz wave. Each plot shows two rf periods (150 ns) at the following times: (**a**) 2 μs, (**b**) 4 μs, (**c**) 10 μs, and (**d**) 50 μs, after the re-ignition start. Each plot is normalized to the value reported in the plot title. Reprinted with permission from [24]. Copyright 2020, American Vacuum Society.

Figure 22 shows the same data but acquired in a discharge pulsed with a wave of 0.1 kHz frequency. While Figure 22a,d show a behavior quite similar to the case of the 10 kHz pulsing frequency, considerable differences can be observed between Figure 22b,c, compared with the corresponding graphs in Figure 21. In fact, during the RF periods represented in these two graphs, the excitation frequency shows two peaks per RF period, as compared to only one observed with the 0.1 kHz pulsing frequency. The stronger of the two peaks happens during the sheath expansion, but the less intense peak is present during the sheath contraction phase. According to the authors' interpretation, this behavior is not consistent with an α heating mode but could be explained considering a hybrid mode involving both α and DA (drift-ambipolar) modes. The latter mode was already introduced

in the case of electronegative gases in a work previously described in this review [17] and could be able to produce the second peak observed. According to these results, it could be possible to tune the electron heating mechanism by changing the pulsing frequency.

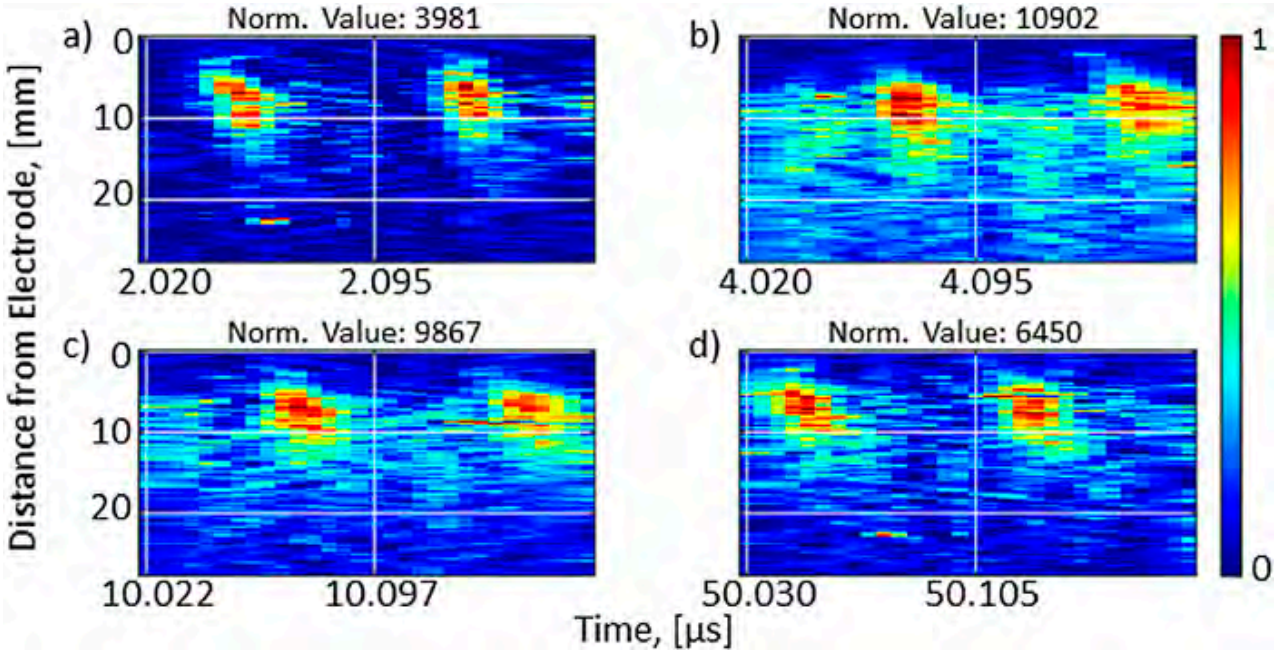

Figure 22. Excitation rate, measured at different times and distances from the powered electrode (at 0 mm) during the re-ignition of an Ar CCP discharge pulsed by a 0.1 kHz wave. Each plot shows two rf periods (150 ns) at the following times: (**a**) 2 μs, (**b**) 4 μs, (**c**) 10 μs, and (**d**) 50 μs, after the re-ignition start. Each plot is normalized to the value reported in the plot title. Reprinted with permission from [24]. Copyright 2020, American Vacuum Society.

Another important work concerning the re-ignition phase in pulsed discharges was published by Wang and coworkers in 2021. Ref. [25] The authors investigated the light emission intensity and the electron density as a function of time in pulsed RF Ar discharges, working at a pressure of 60 Pa and an RF frequency of 12.5 MHz with a steady-state value of the voltage amplitude of 150 V. A rectangular pulsing signal was used, with a T_{ON} fixed at 200 μs and a T_{OFF} varying between 12.5 μs and 800 μs. Figure 23 shows the time evolution of the bias voltage applied on the powered electrode as a function of time for different values of the T_{OFF} time. A different evolution of the bias voltage can be observed in the plot for the different T_{OFF} times during the first 50 μs following the discharge turning off, while after this time the same steady-state value of 150 V is reached for all the plots. This difference in the potential time evolution was explained by the authors considering that, depending on the T_{OFF} time, a different value of the electron density was present in the gas when the discharge was re-activated. Moreover, the V_{RF} value did not drop to zero immediately after the discharge turn off but showed an approximate exponential behavior during about 10 μs, which, according to the authors, was mainly produced by the energy exchange between the discharge and the inductors and capacitors of the matching network.

The time evolution of the light emission intensity and electron density are shown as a function of time in Figure 24 for different values of the T_{OFF} time. The T_N value in the bottom axis of each graph is the number of RF periods: $T_N = t/T_{RF}$, where T_{RF} is the RF period, which is equal to 80 ns with the chosen frequency of 12.5 MHz. As can be seen from Figure 24a,b, the electron density rises to an approximate value of 2×10^9 cm^{-3} after about 25 μs for all the values of the T_{OFF} time considered. After the discharge turns off, the electron density decreases exponentially, as can be seen at t = 200 μs in Figure 24a, down to a minimum density value. As the T_{OFF} value is increased, the electron density decay

rate is increased, while the minimum value it reaches is decreased. The authors attributed these differences to the different behaviors of the neutral atoms with different T_{OFF} times, since if the T_{ON}/T_{OFF} time was longer, the atoms acquired more energy during the T_{ON} time by collision with energetic ions, thus increasing the effective gas temperature and, consequently, reducing its density. A lower neutral gas density would reduce the electron collisions, increasing the probability that they are absorbed by the electrodes.

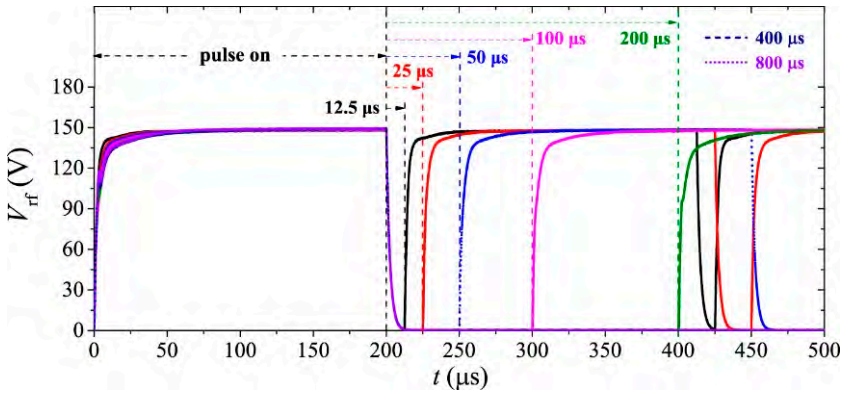

Figure 23. Voltage amplitudes as a function of time in a pulsed RF discharge in Ar working at 60 Pa, for value of the pulse T_{ON} fixed at 200 µs and different values of the pulse T_{OFF}. The vertical dashed lines indicate the times when the next pulse is turned on. Conditions: RF = 12.5 MHz, steady-state rf amplitude V_{steady} = 150 V, T_{ON} = 200 µs, p = 450 mTorr, and L = 2.5 cm. Reprinted from [25] under the terms of Creative Commons Attribution 4.0 license.

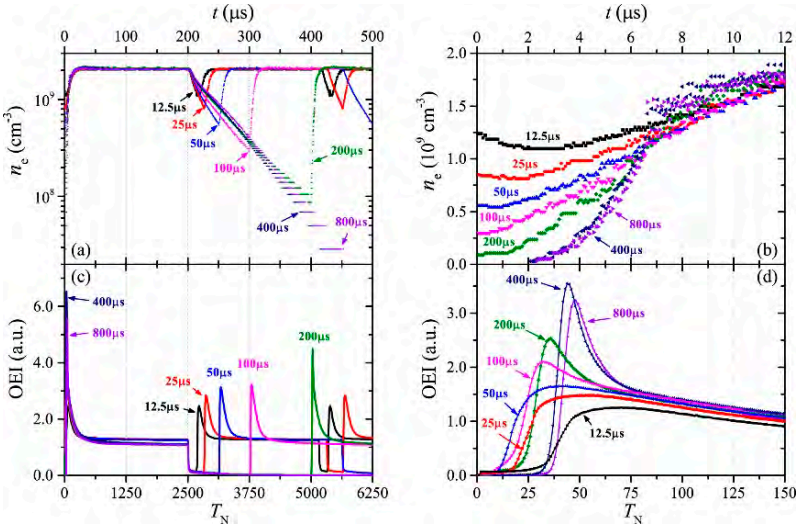

Figure 24. Time evolution of the electron density (**a**,**b**) and optical emission intensity (**c**,**d**) as a function of rf period number T_N, since the beginning of the pulses. $T_N = t/T_{RF}$, where T_{RF} is the duration of one RF period. The labels of the curves specify the T_{OFF} value. Reprinted from [25] under the terms of Creative Commons Attribution 4.0 license.

The time evolution of the light emission intensity is shown in Figure 24c,d, where a sharp peak is visible immediately after the discharge ignition, the intensity of which is enhanced at longer T_{OFF} values. On the other hand, the light emission intensity drops in a much shorter time, compared with the electron density, after the discharge turns off, suggesting that energetic electrons are lost more rapidly than less energetic ones. Figure 24b,d show the time evolution of the electron density and light emission intensity in the first 12 µs after the discharge re-ignition. In Figure 24b, it is clearly visible that the electron density at the beginning of the turn-on phase of the pulse depends strongly on the duration of the turn-off phase, with much higher density values for shorter turn-off times.

According to the authors, this residual electron density has a strong impact on the evolution of the plasma parameters during the discharge re-ignition, as can be seen in Figure 24b,d.

5.5. Step-like Amplitude Modulation in Pulsed Ar Discharges

A less typical type of pulsed discharge, called *step-like amplitude modulation* was applied by Fu and coworkers in 2022 [26] in a CCP-RF discharge working in Ar at 60 Pa, using an electrode distance of 2.5 cm and an excitation frequency of 12.5 MHz. This kind of pulsing involved three different phases during the pulse period, as shown in Figure 25: two phases in which the RF power was active but with different RF amplitudes, and a final phase in which the power was turned off. A first type of pulse, called *step-up* and shown in Figure 25a, had a total duration of 250 µs, during which the signal had a lower amplitude value V_L for the first 100 µs than a higher value V_H for the following 100 µs, and finally was turned off for the last 50 µs. A second type, called *step-down* and shown in Figure 25b, had a total duration of 500 µs, in which the signal intensity was at V_H for the first 100 µs, then at V_L for the following 200 µs, and turned off for the last 200 µs. The value of V_H was fixed at 150 V for both pulse types, while several values of V_L were considered by the authors, corresponding to different values of the voltage ratio $\zeta = V_L/V_H$. For the step-up signal, the values ζ = 0%, 10%, 30%, 50%, 70%, 90%, and 100% were used, while for the step-down modulation, the authors used the values ζ = 0%, 17%, 34%, 50%, 67%, 80%, and 100%.

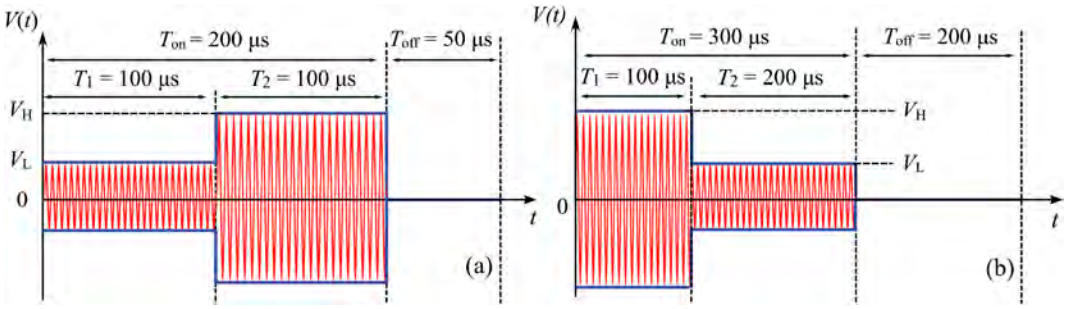

Figure 25. Two different types of step-like amplitude modulation signals used to pulse an RF discharge: (**a**) *step-up* pulse and (**b**) *step-down* pulse. © IOP Publishing. Reproduced from [26] with permission. All rights reserved.

Figure 26 shows the time evolution of the electron density in the discharge during the different phases of the step-up (Figure 26a) and step-down (Figure 26b) pulse types for different values of the voltage ratio ζ. In the case of the step-up pulse signal, shown in Figure 26a, the electron density shows a similar behavior for all the pulses with a voltage ratio $\zeta \geq 50\%$, for which a step-like increase can be observed during the first part of the pulse, followed by a second increase during the second part, and a decrease in the last part, in which, however, the electron density does not reach zero. For lower values of the voltage ratio ζ, the time evolution of the electron density becomes more complex, with two peaks, shown by pink arrows in Figure 26a, in the case of ζ = 30% and a single peak at 50 µs for ζ = 10%. The authors provided a complex explanation for this behavior, which is too long to be reported here. In the case of the step-down pulse signal, shown in Figure 26b, the time evolution of the electron density during the first part of the pulse is identical for all the values of the voltage ratio ζ, showing a step-like increase to the same value. During the second part of the pulse, the behavior is similar for $\zeta \geq 50\%$, with a step-like reduction, which becomes negligible for ζ = 100%, where there is no step-down between the two pulse phases. The behavior is more complex for $\zeta < 50\%$, with the formation of a double step for ζ = 34% and a density peak at 200 µs for ζ = 17%. It is also interesting to note that the electron density decreases faster to a zero value for ζ = 17% compared with the case of ζ = 0%. The authors also provided an interesting explanation for these behaviors, which, however, is too long to be included in this review.

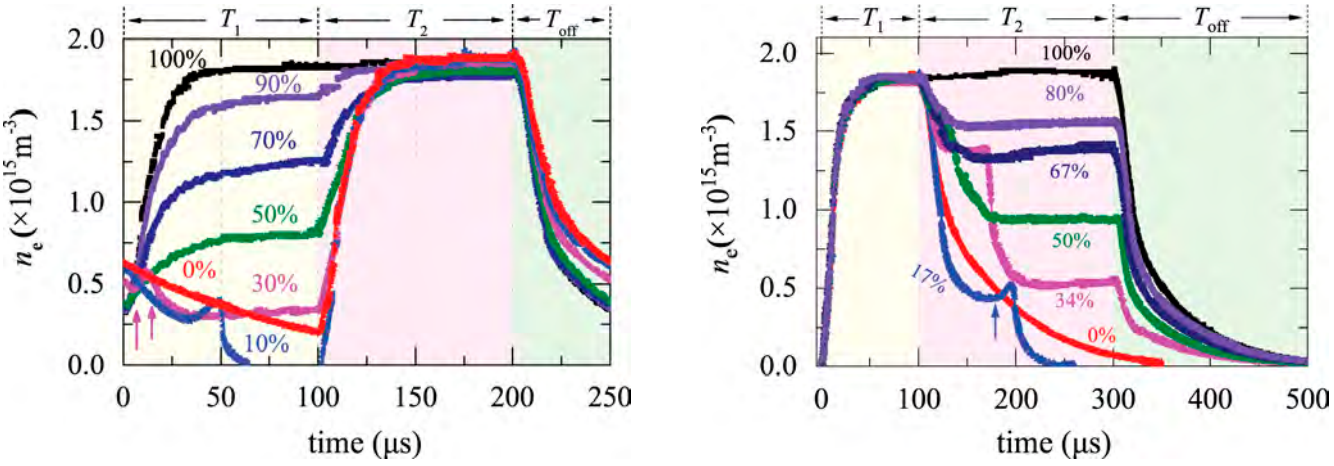

Figure 26. Time evolution of the electron density in an RF-CCP Ar discharge working at 60 Pa, pulsed by means of the (**a**) *step-up* and (**b**) *step-down* pulse types shown in Figure 25a and Figure 25b respectively. The percentage values near the curves represent the values of the voltage ratio voltage ratio $\zeta = V_L/V_H$. © IOP Publishing. Reproduced from [26] with permission. All rights reserved.

5.6. Time Evolution of Ion Properties in Pulsed Discharges Using Ar + C_2H_2 Mixture

Most of the research papers reviewed here deal with the time evolution of electron properties, but the time evolution of ions and neutrals is also important for investigating the discharge behavior. In this context, an interesting paper concerning the time evolution of both charged and neutral species in a discharge composed by Ar and C_2H_2 was published in 2022 by Jimenez-Redondo and coworkers. Ref. [27] The authors investigated the time evolution of the density of several charged and neutral radicals using a combination of mass spectrometry and a 0D kinetic model consisting of a time-dependent differential equation for each species. The discharge was characterized by a 13.56 MHz RF frequency, a gas flow ratio $[C_2H_2]/[Ar] = 1.25$, and a pulsing frequency of 100 Hz with a 50% duty cycle. Figure 27 shows the neutral densities of Ar atoms and several dissociation and recombination byproducts inside the discharge. The values shown in Figure 27a,b were obtained from the kinetic model using experimental data measured by means of a quadrupole mass spectrometer and a plasma process monitor, respectively. According to the authors, the latter was used for the lighter species due to its better signal-to-noise ratio. An increase in the hydrogen density, which was produced by the dissociation of C_2H_2 molecules in in the discharge, is clearly visible in the plot up to the final steady-state. The densities of carbon-based radicals, instead, follow a different type of evolution, with a steep rise to a peak value, followed by a slow decrease. The time evolution of several cation densities is shown in Figure 28, where a continuous increment with time of Ar^+ and ArH^+ is clearly visible, up to a steady-state value. On the other hand, the densities of cations of carbon-based radicals show a peak at different times during the first 10 s of the discharge, resembling the behavior of carbon-neutral species. Figure 29 shows the time-dependent density of several anions, among which the C_2H^- shows a peculiar behavior, compared to the other cations, with a continuous rise to the steady state, instead of showing a minimum at about 30 s. The authors attributed this difference to the different formation mechanisms of the cations, where C_2H^- was produced by direct electron attachment, while the other cations were formed during chemical reactions in the discharge.

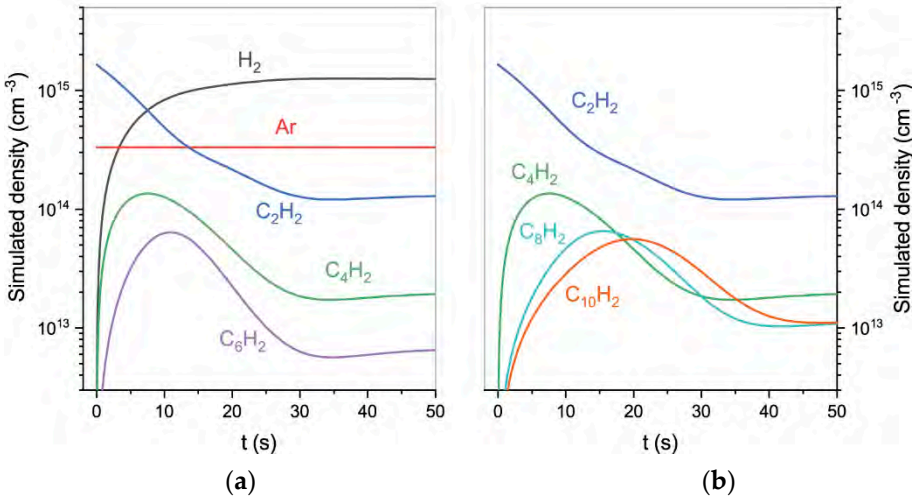

Figure 27. Time evolution of the density of several neutral species in an Ar+C_2H_2 RF pulsed discharge, obtained by a 0D kinetic simulation based on the experimental data obtained by (**a**) a mass spectrometer and (**b**) a plasma process monitor. © IOP Publishing. Reproduced from [27] with permission. All rights reserved.

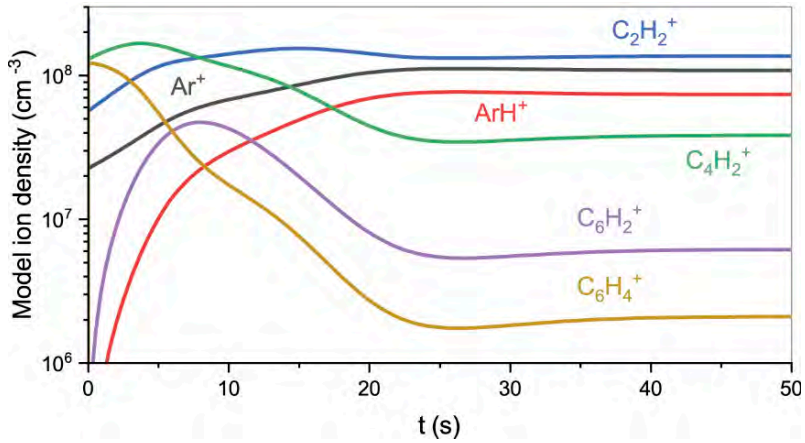

Figure 28. Time evolution of the density of several cations in an Ar+C_2H_2 RF pulsed discharge, obtained by a 0D kinetic simulation based on the experimental data obtained by a plasma process monitor. © IOP Publishing. Reproduced from [27] with permission. All rights reserved.

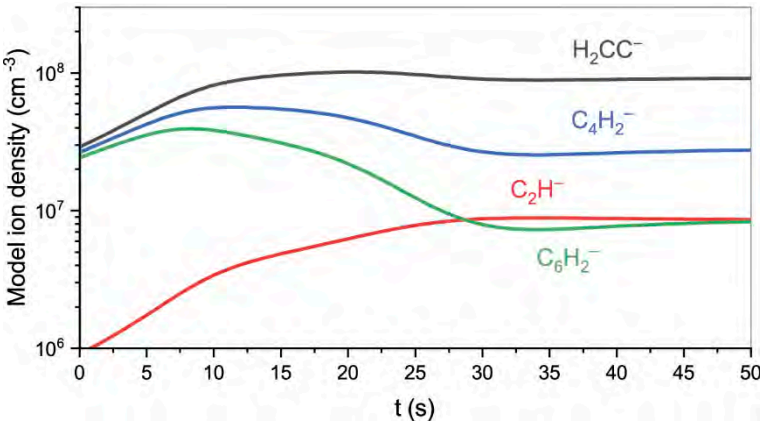

Figure 29. Time evolution of the density of several anions species in Ar+C_2H_2 RF pulsed discharge, obtained by a 0D kinetic simulation based on the experimental data obtained by a plasma process monitor. © IOP Publishing. Reproduced from [27] with permission. All rights reserved.

5.7. Time Evolution of Ion Properties in Pulsed Discharges Using Ar + C_4F_8 + O_2 Mixture

The last work dealing with pulsed discharges included in this review, which was published in 2023 by Kuboi and coworkers, ref. [28] deals with the time-resolved analysis of the positive ion density in a pulsed dual-frequency RF-CCP discharge, working with a mixture of Ar, C_4F_8, and O_2 at a pressure of 4 Pa. One of the electrodes was powered simultaneously by a VHF and LF signal working at different frequencies and powers, both pulsed with the same pulsing wave. The VHF signal had a frequency of 40 MHz and a power of 100 W, while the LF signal had a 2 MHz frequency and 20 W power. The pulsing was achieved by a rectangular wave with a 1 kHz frequency and a 50% duty cycle. The authors measured the densities of ion species through a QMS, and applied specific normalization procedures, not reported here for space limitations, to overcome the issues related to the measurement of the volume density from the mass spectrum. Figure 30a shows the time evolution of the cation density in a discharge composed by Ar only, which was used as a reference to which the more complex gas mixture discharge was compared. The Ar^+ density required more than 100 μs to reach the steady state, then started to drop at 500 μs when the turn-off phase of the pulse started, reaching a zero density in about 100 μs. Figure 30b shows the time-resolved densities of several cations in the Ar + C_4F_8 + O_2 discharge, where a completely different behavior of the Ar^+ density can be observed, with an immediate drop at the pulse turn-on, which lasts about 100 μs, followed by a gentler reduction, which lasts until the start of the turn-off phase of the pulse. During the intermediate part of the turn-on phase the most intense density is observed for the C_2F_4, cations, while O_2^+ density remains very low for the entire pulse duration. The authors measured the time-resolved electron density during the first 40 μs of the pulse, and Figure 31 reports this result, together with the calculated ratio between the Ar^+ and electron densities, which the authors considered an estimation of the electron temperature. This ratio showed a rapid fall during the first few microseconds of the pulse, then continued to reduce more slowly until it reached a steady state after about 3 μs, while the electron temperature rose more slowly and reached a constant value at about the same time. The authors noted that the intensity of charge species showed a time evolution even after the time required to stabilize electron density and temperature and proposed a model to justify this behavior. The time evolution of charged species is of considerable importance in reactive ion etching (RIE) applications, especially when high aspect ratio geometries are required, considering that the etching process at the bottom of trenches is mainly due to reactive ions since neutral radicals usually do not have the energy required to reach the bottom surfaces.

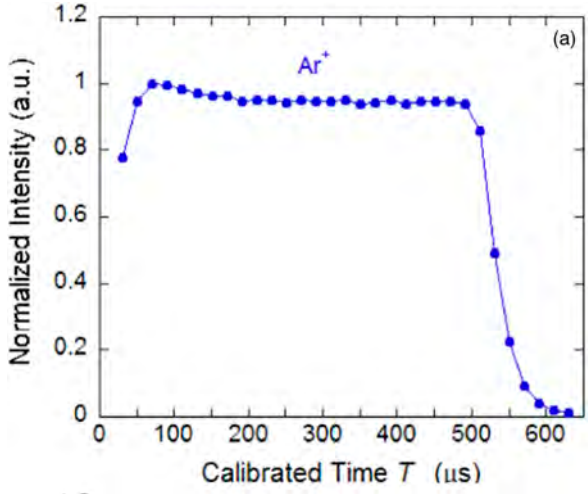

Figure 30. *Cont.*

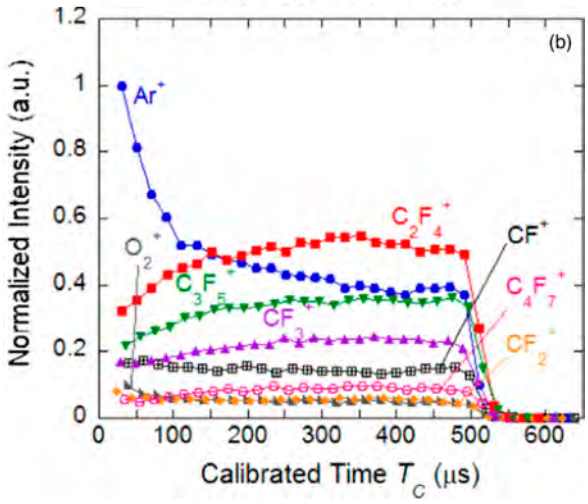

Figure 30. Time evolution of the density of Ar^+ and other anions in pulsed double-frequency RF discharges composed by (**a**) Ar only and (**b**) an $Ar+C_4F_8+O_2$ gas mixture. © The Japan Society of Applied Physics. Reproduced from [28] by permission of IOP Publishing Ltd. All rights reserved.

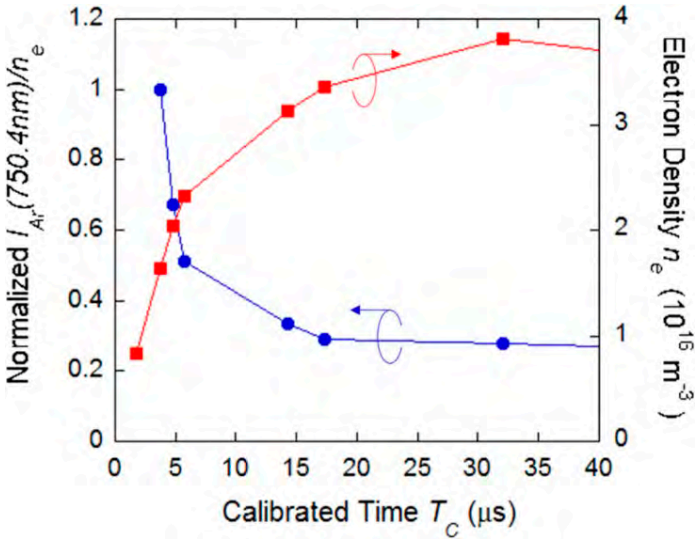

Figure 31. Time evolution of the electron density (in red, right scale) and Ar density normalized to the electron density (in blue, left scale) in a pulsed double-frequency RF discharges composed by an $Ar + C_4F_8 + O_2$ gas mixture. © The Japan Society of Applied Physics. Reproduced from [28] by permission of IOP Publishing Ltd. All rights reserved.

6. Effect of Parasitic Discharges in the Time Evolution of Plasma Parameters

6.1. Plasmoid Formation in H_2 Discharges

An interesting phenomenon that may appear in plasma discharges is the *plasmoid*, which consists of a localized, small volume of plasma, associated with a light emission significantly more intense than its surroundings and is associated with much greater values of several plasma parameters, such as electron density and temperature. Plasmoids can sometimes be observed near the powered electrodes of plasma discharges, especially in the case of structured, grid-shaped electrodes. An interesting work on this subject was published by Chesaux and coworkers in 2013, ref. [29] in which the authors measured, by means of PROES, the time-resolved Hα emission (656 nm) from plasma near a grid positioned in the middle of a CCP reactor, parallel to the grounded electrode, during an RF (13.56 MHz) discharge in H_2 at 100 Pa, working in normal conditions, and during the formation of a plasmoid. Figure 32a shows the emission intensity as a function of time

and the distance from the grid, which is shown as a blue bar, while Figure 32b shows the corresponding time evolution of the RF bias applied at the powered electrode. Two peaks of light emission are visible at about 5 ns and 45 ns: the former is addressed by the authors to the acceleration of electrons towards the RF electrodes, while the latter is considered due to the ejection of electrodes from the electrode toward the grid. The latter is consistent with similar measurements made in 1998 by Czarnetzki and coworkers [14], who observed a peak of emission intensity at about 45 ns in a similar H_2 discharge, although in that case there was no grid positioned in the discharge volume. The dashed arrows shown in the figure and labeled as I and II indicate the presumed direction of the electron motion. The discharge is confined in the region between the grid and the powered electrode (upper region in the image), but a low emission is also observed between the grid and the grounded electrode, which is addressed by the authors to the electrons pushed from the cathode and penetrating the grid. Figure 33 shows the same arrangement in conditions where a plasmoid is generated just above the grid. A peak of emission intensity is visible just below the grid, close to the time at which the maximum bias is reached and is attributed by the authors to a current flowing back from the grounded electrode to the powered one and passing through the grid. Another intensity peak is visible at about 30 ns and is quite similar to the one observed without the plasmoid.

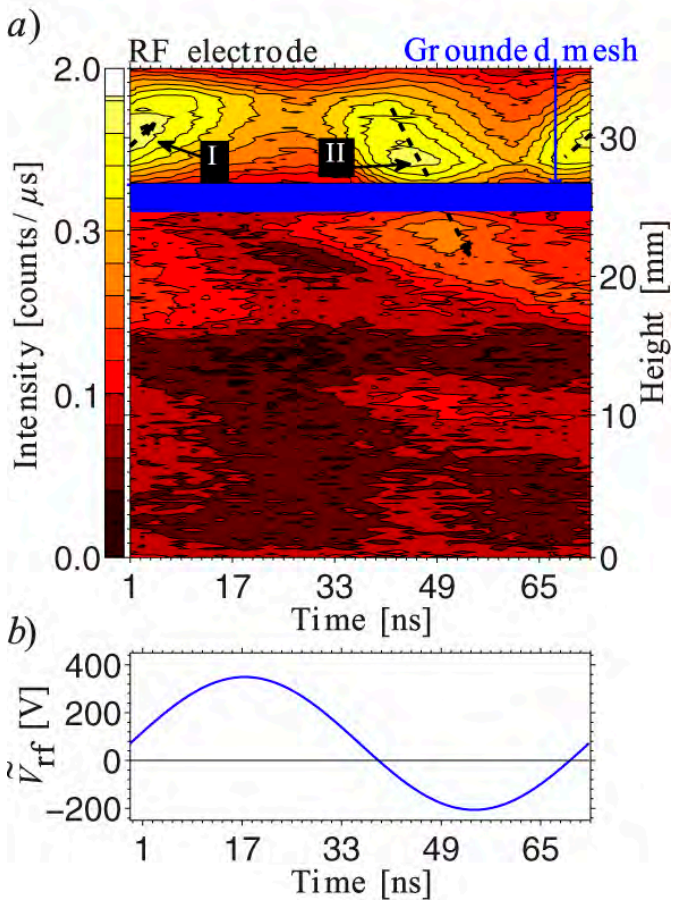

Figure 32. (**a**) Emission intensity of the Hα line, as a function of time and vertical position, in an H_2 discharge working at 100 Pa without plasmoids, near a grid positioned parallel to the electrodes. The dashed arrows, marked I and II, show the expected direction of electron flows. (**b**) Voltage on the rf electrode. The color scale is logarithmic. © IOP Publishing. Reproduced with permission from [29]. All rights reserved.

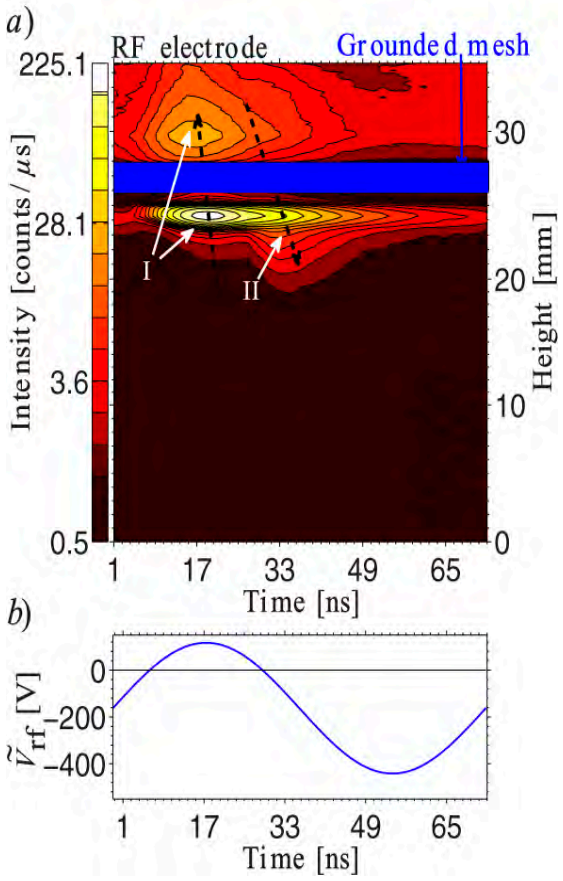

Figure 33. (**a**) Emission intensity of the Hα line, as a function of time and vertical position, in a H_2 discharge working at 100 Pa with a plasmoid, near a grid positioned parallel to the electrodes. The dashed arrows, marked I and II, show the expected direction of electron flows. (**b**) Voltage on the rf electrode. The color scale is logarithmic. © IOP Publishing. Reproduced with permission from [29]. All rights reserved.

6.2. Micro-Arc Discharges Formation in Ar Discharges with Oil-Coated Electrodes

A problem that may arise in plasma CCP discharges is the formation of localized micro-arc discharges, usually in proximity of one of the electrodes. These phenomena may be detrimental since they can produce damage to the material under treatment or to the reactor. This subject was addressed by Kim and coworkers in a 2015 study, ref. [30] in which some results were reported about the time-dependent variations of the floating potential near the oil-coated surface of the grounded electrode in an RF-CPP discharge, working in Ar at a pressure of 6.66 Pa and an applied power in the range 10–100 W. The authors used an unusual configuration, in which a shunt inductor was inserted between the powered electrode and the RF generator. A fraction of the grounded electrode surface was covered by a thin layer of oil before the discharge ignition. The authors reported that the micro-arcs were observed only near the oil-coated regions of the electrode and were shorter than the sheath length. Figure 34 shows the floating potential, measured by means of a Langmuir probe, immediately before and during the formation of a micro-arc when a power of 50 W was applied to the electrode. A sudden drop of the floating potential immediately after the micro-arc ignition can be observed in the plot, followed by a linear increase in its intensity. According to the authors, the potential drop happens in a time of about 200 ns, while the original potential value is restored after about 20 μs, as can be seen in the figure. According to the authors' interpretation, the oil vapors emitted from the oil-coated regions of the electrode surface play an important role in the micro-arc formation.

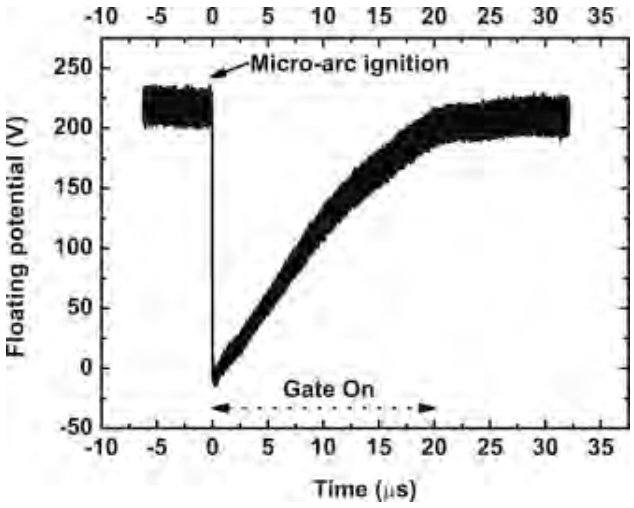

Figure 34. Floating potential, measured during the ignition of a micro-arc discharge, near the oil-coated surface of the grounded electrode, in an RF-CCP discharge in Ar at 6.66 Pa and 50 W of applied RF power. Reprinted from [30], Copyright (2015), with permission from Elsevier.

7. Other Topics

7.1. Influence of Powder Formation in Discharges Using Ar + C_2H_2 Mixture

An important phenomenon that may take place in some kinds of plasma discharges at certain conditions is the formation of dust particles. This effect is usually unwanted during plasma-assisted deposition or etching processes since dust particles can contaminate the material under treatment or be incorporated into the growing lattice, but they can be exploited for the production of nanoparticles. An interesting work about this subject was published in 2017 by Stefanović and coworkers [31], in which the electron and excited metastable Ar atom density was measured as a function of time during RF (13.56 MHz) continuous and pulsed CCP discharges using mixtures of Ar and C_2H_2. The authors investigated the plasma discharge behavior in four conditions: Ar-only discharge; Ar plus C_2H_2 before and during the formation of dust particles; and pure Ar plasma with dust, achieved by suppressing the C_2H_2 flow after the particles had been formed. The density of metastable Ar atoms was measured by means of *laser absorption spectroscopy* (LAS) at 772.38 nm, while the electron density was measured by *microwave interferometry* (MIW).

When the discharge was activated in continuous mode, without pulsing, in a mixture of Ar and C_2H_2, the formation of dust particles was observed, which grew in size up to an approximate average dimension of 0.6 μm, then were removed from the plasma region due to the electrostatic forces. At that point, the formation of new particles started, giving rise to a series of cycles of particle formation and expulsion. The electron density in the plasma discharge as a function of time during two of these cycles is shown in Figure 35, where a considerable reduction of the electron density is visible during the dust growth cycles. According to the authors' interpretation, the surfaces of dust particles collect a considerable fraction of the plasma electrons during their growth, thus reducing the plasma density.

The authors also investigated the dust formation when pulsing the discharge and found that the pulsing frequency could be used to activate or suppress the dust formation in the Ar + C_2H_2 mixture since the phenomenon was inhibited for frequencies lower than 700 Hz. Figure 36 shows the densities of Ar metastables and electrons measured as a function of time in a discharge in Ar and acetylene at a pressure of 0.1 mbar and power of 40 W, pulsed by a signal with a 100 Hz frequency and a 50% duty cycle. The different lines and symbols represent different gas mixtures, as described in the figure caption, and the graph shows considerably different behaviors of the two plasma parameters depending on the composition.

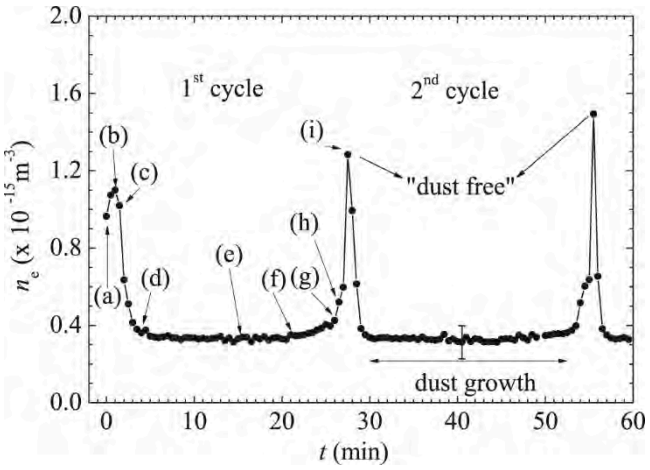

Figure 35. Electron density in a plasma discharge in Ar and C_2H_2 measured during two consecutive cycles of dust formation. The letters in the graph refer to different stages of the cycle: (a) t = 0 min plasma ignition in pure argon, (b) t = 1.1 min injection of acetylene, (c) t = 1.7 min starting of dust formation, (d) t = 3.9 min maximum plasma emission in the discharge, (e) t = 15.7 min, (f) t = 21.7 min, (g) t = 26.65 min, (h) t = 27.08 min particle expulsion from the plasma region, (i) t = 27.3 min starting of a new particle growth cycle. © IOP Publishing. Reproduced with permission from [31]. All rights reserved.

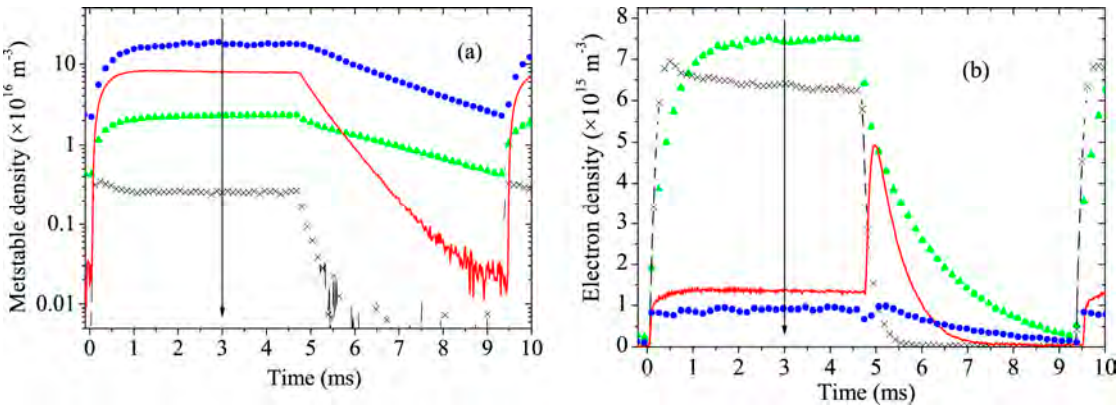

Figure 36. (**a**) Density of metastable excited Ar atoms and (**b**) electron density, measured as a function of time in a pulsed plasma discharge in Ar and C_2H_2 at 0.1 mbar and 40 W. Different gas mixtures are represented by different symbols on the graph: solid green triangles for pure Ar, black crosses for Ar + C_2H_2, solid red line for Ar + C_2H_2 with dust, and blue dotted line for Ar with dust. © IOP Publishing. Reproduced with permission from [31]. All rights reserved.

7.2. Time-Dependent Gas Mixture Composition in Discharges Using Ar + N_2 + C_6H_{14} Gas Mixture

The time-dependent behavior of several plasma parameters when other gases are injected in an Ar RF-CCP discharge was investigated by Ogawa and coworkers in an interesting work published in 2010. Ref. [32] The authors studied the injection of Ar, N_2, as well as hexane, in both gaseous and bubble form, inside an Ar discharge and monitored the time evolution of several parameters, including electron density and temperature, as well as light emission. Figure 37 shows the time evolution of several parameters after the injection of hexane gas inside an Ar RF-CCP discharge working at a pressure of 23 Pa and an RF power of 7 W. The matching network parameters were previously tuned to minimize the reflected RF power in a mixture of Ar and hexane, so the reflected power shown in Figure 37a at t = 0 ms is quite high since, before the hexane injection, a discharge of pure Ar was present in the reactor, and the matching network tuning was not optimized for it. After the hexane injection, a decrease in the reflected power can be observed in the plot, which

becomes negligible after about 60 ms, while the net power increases, reaching a final value of about 10 W after 100 ms. Figure 37b shows the time evolution of the plasma density and electron temperature after the hexane injection. The former was measured by means of microwave interferometry (MWI), shown as a continuous line in Figure 37b, which provided a measure of the electron density weighted over all the reactor volume, and by a Langmuir probe of wise type, shown as a dashed line, which provided a localized signal related to a small volume near the powered electrode. As can be seen from Figure 37b, the localized plasma density remained practically constant after the injection, and the space-averaged one showed a relatively modest increase. On the other hand, a substantial reduction of the electron temperature can be observed in the graph, especially during the first 10 ms after the hexane injection. The authors suggest that this behavior could be related to the different ionization potentials of hexane and its dissociation products compared with Ar, as well as to the electron energy absorbed by vibrational and rotational excitations of hexane. Figure 37c,d show the optical emission of plasma at 415.9 nm, which is related to Ar, and 431.4 nm, which relates to CH radicals, measured in 4 different regions of the discharge. The Ar emission is reduced after the hexane injection, and the authors address the Penning ionization by means of Ar* metastable excited atoms as one of the most probable causes. On the other hand, the CH emission from the region near the cathode (line 4) remains approximately constant and does not change with the hexane injection. According to the authors' interpretation, this emission is not due to hexane dissociation byproducts but rather to radicals produced from the interaction between the plasma and the electrode surface.

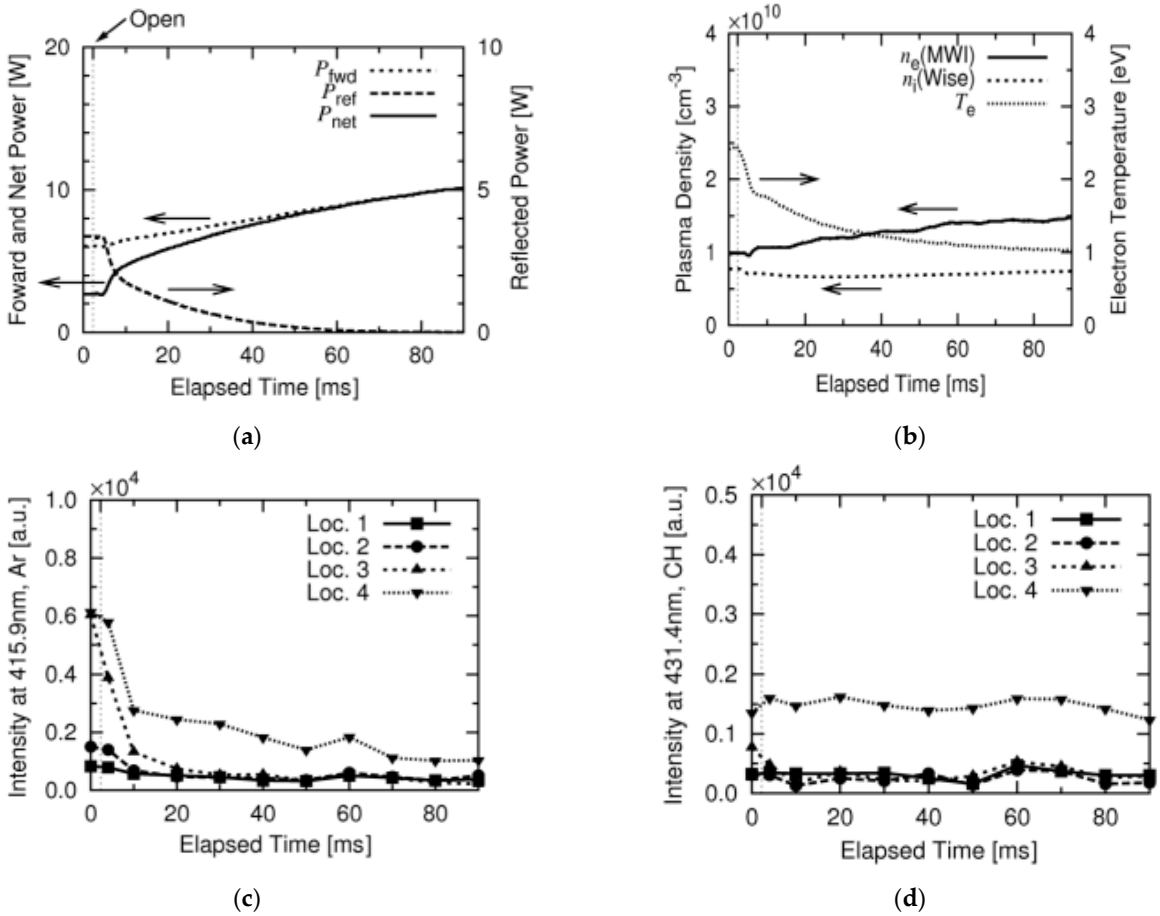

Figure 37. Forward, reflected, and net power (**a**); electron density and temperature (**b**); and light emission intensity at 415.9 nm (**c**) and at 431,4 nm (**d**) as a function of time after the injection of hexane gas in an Ar discharge. Reproduced with permission from [32]. All rights reserved.

7.3. Effects of Surface Erosion

RF-CCP plasma discharges are often used for the physico-chemical modification of surfaces, such as in sputtering and plasma etching processes, thanks to their ability to provide an ion bombardment and to deliver reactive radicals to the surface of materials. The material removed from the surface in contact with the discharge can be incorporated into the discharge composition and give rise to a substantial modification of its behavior. In some cases, unwanted etching effects are also possible in discharges that are activated for other purposes. An example of this kind of effect is reported in a study from Sackers and coworkers of 2022, ref. [33] related to the problem of the removal of metallic atoms from the inner surfaces of a fusion reactor due to the etching exerted by the fusion plasma and the subsequent deposition of the same elements on the surface of metallic mirrors used inside the reactor. The authors studied the possibility of cleaning the contaminated surfaces by means of an RF-CPP Ar discharge working at 60 MHz with pressures in the range of 0.5–10 Pa and power in the range 20–100 W. The unusual excitation frequency was chosen to reduce the sheath thickness, in order to limit the ion bombardment energy, and to prevent unwanted interferences with the excitation frequencies of the *ion cyclotron resonance* (ICR) devices used to light the fusion plasma. The work does not provide experimental or calculation results about the time evolution of plasma quantities; however, it provides an extensive investigation of the effects of plasma conditions on several plasma parameters.

8. Conclusions

In this work, a review was presented concerning the main experimental research works focused on the time evolution of one or more plasma parameters in low-pressure, capacitively coupled radio frequency discharges. The reviewed works cover a time span from 1989 to 2023, and each of them contains experimental results about the time evolution of one or more plasma parameters, while some also include simulation or analytical results. Table 1 summarizes, for each paper, the physical quantities for which the time evolution was considered and reports the time scale, defined as the time span over which the results are presented, as well as the time resolution. Most of the reviewed works deal with Ar-based discharges, but a few of them include other types of gases, including He, Ne, and H_2, as well as hydrocarbons or even fluorine-based discharges.

Table 1. List of the plasma parameters measured or calculated as a function of time in the reviewed articles.

Time Resolution [2]	Time Scale [1]	Plasma Parameters	Plasma Composition	Refs.
N/A [3]	10^{-8} s	Plasma potential (V_p) Electron temperature (kT_e) Electron density (n_e)	Ar	[11]
N/A	10^{-7} s	Probe voltage	Ar	[12]
10^{-7} s	10^{-3} s	Discharge voltage (V_e) Discharge current (I_e) Discharge RF power (P) Electron density (n_e) Collision frequency (f)	Ar	[14]
10^{-4} s	10^{-2} s	Electron density Electron temperature	He, Ar	[15]
10^{-8} s	10^{-7} s	Voltage over the sheaths	He, H_2	[16]
10^{-8} s	10^{-7} s	Rotational temperature of H_2	H_2	[17]
10^{-6} s	10^{-3} s	Electron density Optical emission intensity	Ar	[18]

Table 1. *Cont.*

Time Resolution [2]	Time Scale [1]	Plasma Parameters	Plasma Composition	Refs.
10^{-3} s	10^{-1} s	Electron temperature Electron density Light emission	Ar, N_2, C_6H_{14}	[19]
10^{-8} s	10^{-9} s	Ionization rate Light emission intensity	CF_4	[20]
10^{-7} s	10^{-9} s	Excitation rate of Ne	Ne	[21]
10^{-9} s	10^{-7} s	Light emission intensity	H_2	[22]
10^{-7} s	10^{-4} s	Floating potential	Ar	[23]
10^{-5} s	10^{-2} s	Ar metastable density Electron density	Ar, C_2H_2	[24]
10^{-6} s	1 s	Light emission intensity	Ar	[25]
10^{-8} s	10^{-7} s	Excitation rate	Ar	[26]
10^{-7} s	10^{-5} s	Electron density Light emission intensity	Ar	[27]
10^{-7} s	10^{-5} s	Electron density Light emission intensity	Ar	[28]
10^{-6} s	10^{-3} s	Electron density	Ar	[29]
1 s	10^2 s	Neutral density (Ar, H_2, C_2H_2, C_4H_2, C_6H_2, C_8H_2, $C_{10}H_2$) Cation density (Ar^+, $C_2H_2^+$, $C_4H_2^+$,$C_6H_2^+$, $C_6H_4^+$) Anion density (H_2CC^-, C_2H^-, $C_4H_2^-$, $C_6H_2^-$)	Ar, C_2H_2	[30]
10^{-5} s	10^{-3} s	Cation density (Ar^+, O_2^+, CF^+, CF_2^+, CF_3^+, $C_2F_4^+$, $C_3F_5^+$, $C_4F_7^+$)	Ar, C_4F_8, O_2	[31]

[1] Order of magnitude of the larger time span among all the measurements reported in the paper. [2] Order of magnitude of the better resolution among all the measurements reported in the paper. [3] N/A indicates that the value cannot be obtained from the data provided or is too uncertain.

Several papers refer to the *GEC reference cell*, the design of which was started by an ad hoc committee formed at the 1988 Gaseous Electronics Conference and was finally published as a reference standard in 1994 [11]. Earlier papers provide results with a lower time resolution, while works published in recent years report results with resolution in the nanosecond range. An important topic, which is addressed in several of the reviewed papers, is the development of a model to explain the behavior of pulsed discharges, especially considering the re-ignition phase, when the RF bias turns on after being suppressed during the turn-off part of the pulse. In fact, the discharge behavior during this phase was found to be strongly dependent on the duration of the turn-off part of the pulse. While several authors presented interesting experimental data about the time evolution of electron density and temperature during the re-ignition phase, the discharge behavior during the first two microseconds has not yet been measured due to the limitations of available experimental apparatuses, with only simulation data available.

Funding: This research received no external funding.

Conflicts of Interest: The author declares no conflicts of interest.

References

1. von Keudell, A.; Schulz-von der Gathen, V. Foundations of Low-Temperature Plasma Physics—An Introduction. *Plasma Sources Sci. Technol.* **2017**, *26*, 113001. [CrossRef]
2. Ostrikov, K.; Xu, S.; Huang, S.Y.; Levchenko, I. Nanoscale Surface and Interface Engineering: Why Plasma-Aided? *Surf. Coat. Technol.* **2008**, *202*, 5314–5318. [CrossRef]
3. Marchack, N.; Buzi, L.; Farmer, D.B.; Miyazoe, H.; Papalia, J.M.; Yan, H.; Totir, G.; Engelmann, S.U. Plasma Processing for Advanced Microelectronics beyond CMOS. *J. Appl. Phys.* **2021**, *130*, 080901. [CrossRef]
4. Xiao, S.Q.; Xu, S.; Ostrikov, K. Low-Temperature Plasma Processing for Si Photovoltaics. *Mater. Sci. Eng. R Rep.* **2014**, *78*, 1–29. [CrossRef]
5. Granqvist, C.G. Electrochromics for Smart Windows: Oxide-Based Thin Films and Devices. *Thin Solid Film.* **2014**, *564*, 1–38.
6. Hammer, T. Atmospheric Pressure Plasma Application for Pollution Control in Industrial Processes. *Contrib. Plasma Phys.* **2014**, *54*, 187–201. [CrossRef]
7. Weltmann, K.-D.; von Woedtke, T. Plasma Medicine—Current State of Research and Medical Application. *Plasma Phys. Control. Fusion* **2016**, *59*, 014031. [CrossRef]
8. Chabert, P.; Tsankov, T.V.; Czarnetzki, U. Foundations of Capacitive and Inductive Radio-Frequency Discharges. *Plasma Sources Sci. Technol.* **2021**, *30*, 024001. [CrossRef]
9. Mandracci, P.; Rivolo, P. Recent Advances in the Plasma-Assisted Synthesis of Silicon-Based Thin Films and Nanostructures. *Coatings* **2023**, *13*, 1075. [CrossRef]
10. Carneiro de Oliveira, J.; Airoudj, A.; Kunemann, P.; Bally-Le Gall, F.; Roucoules, V. Mechanical Properties of Plasma Polymer Films: A Review. *SN Appl. Sci.* **2021**, *3*, 656. [CrossRef]
11. Hargis, P.J., Jr.; Greenberg, K.E.; Miller, P.A.; Gerardo, J.B.; Torczynski, J.R.; Riley, M.E.; Hebner, G.A.; Roberts, J.R.; Olthoff, J.K.; Whetstone, J.R.; et al. The Gaseous Electronics Conference Radio-frequency Reference Cell: A Defined Parallel-plate Radio-frequency System for Experimental and Theoretical Studies of Plasma-processing Discharges. *Rev. Sci. Instrum.* **1994**, *65*, 140–154. [CrossRef]
12. Wilson, J.L.; Caughman, J.B.O., II; Nguyen, P.L.; Ruzic, D.N. Measurements of Time Varying Plasma Potential, Temperature, and Density in a 13.56 MHz Radio-frequency Discharge. *J. Vac. Sci. Technol. A* **1989**, *7*, 972–976. [CrossRef]
13. Wood, B.P.; Lieberman, M.A.; Lichtenberg, A.J. Sheath Motion in a Capacitively Coupled Radio Frequency Discharge. *IEEE Trans. Plasma Sci.* **1991**, *19*, 619–627. [CrossRef]
14. Czarnetzki, U.; Luggenhölscher, D.; Döbele, H.F. Space and Time Resolved Electric Field Measurements in Helium and Hydrogen RF-Discharges. *Plasma Sources Sci. Technol.* **1999**, *8*, 230. [CrossRef]
15. Sun, G.-Y.; Sun, A.-B.; Zhang, G.-J. Intense Boundary Emission Destroys Normal Radio-Frequency Plasma Sheath. *Phys. Rev. E* **2020**, *101*, 033203. [CrossRef]
16. Gans, T.; der Gathen, V.S.; Döbele, H.F. Time Dependence of Rotational State Populations of Excited Hydrogen Molecules in an RF Excited Plasma Reactor. *Plasma Sources Sci. Technol.* **2001**, *10*, 17. [CrossRef]
17. Schulze, J.; Derzsi, A.; Dittmann, K.; Hemke, T.; Meichsner, J.; Donkó, Z. Ionization by Drift and Ambipolar Electric Fields in Electronegative Capacitive Radio Frequency Plasmas. *Phys. Rev. Lett.* **2011**, *107*, 275001. [CrossRef] [PubMed]
18. Schmidt, N.; Schulze, J.; Schüngel, E.; Czarnetzki, U. Effect of Structured Electrodes on Heating and Plasma Uniformity in Capacitive Discharges. *J. Phys. D Appl. Phys.* **2013**, *46*, 505202. [CrossRef]
19. Su, Z.-X.; Shi, D.-H.; Liu, Y.-X.; Zhao, K.; Gao, F.; Wang, Y.-N. Radially-Dependent Ignition Process of a Pulsed Capacitively Coupled RF Argon Plasma over 300 Mm-Diameter Electrodes: Multi-Fold Experimental Diagnostics. *Plasma Sources Sci. Technol.* **2021**, *30*, 125013. [CrossRef]
20. Overzet, L.J.; Leong-Rousey, F.Y. Time-Resolved Power and Impedance Measurements of Pulsed Radiofrequency Discharges. *Plasma Sources Sci. Technol.* **1995**, *4*, 432. [CrossRef]
21. Overzet, L.J.; Kleber, J. Effect of Metastable Atom Reactions on the Electron Energy Probability Functions in Afterglows. *Plasma Sources Sci. Technol.* **1998**, *7*, 512. [CrossRef]
22. Šamara, V.; Bowden, M.D.; Braithwaite, N.S.J. Effect of Power Modulation on Properties of Pulsed Capacitively Coupled Radiofrequency Discharges. *J. Phys. D Appl. Phys.* **2010**, *43*, 124017. [CrossRef]
23. Lee, Y.; Song, W.; Hong, S.J. In Situ Monitoring of Plasma Ignition Step in Capacitively Coupled Plasma Systems. *Jpn. J. Appl. Phys.* **2020**, *59*, SJJD02. [CrossRef]
24. Hernandez, K.; Overzet, L.J.; Goeckner, M.J. Electron Dynamics during the Reignition of Pulsed Capacitively-Coupled Radio-Frequency Discharges. *J. Vac. Sci. Technol. B* **2020**, *38*, 034005. [CrossRef]
25. Wang, X.-Y.; Liu, J.-R.; Liu, Y.-X.; Donkó, Z.; Zhang, Q.-Z.; Zhao, K.; Schulze, J.; Wang, Y.-N. Comprehensive Understanding of the Ignition Process of a Pulsed Capacitively Coupled Radio Frequency Discharge: The Effect of Power-off Duration. *Plasma Sources Sci. Technol.* **2021**, *30*, 075011. [CrossRef]
26. Fu, Y.-Y.; Wang, X.-K.; Liu, Y.-X.; Schulze, J.; Donkó, Z.; Wang, Y.-N. Effects of 'Step-like' Amplitude-Modulation on a Pulsed Capacitively Coupled RF Discharge: An Experimental Investigation. *Plasma Sources Sci. Technol.* **2022**, *31*, 085005. [CrossRef]
27. Jiménez-Redondo, M.; Tanarro, I.; Herrero, V.J. Time Evolution of Neutral and Charged Species in Ar/C2H2 Capacitively-Coupled RF Discharges. *Plasma Sources Sci. Technol.* **2022**, *31*, 065003. [CrossRef]

28. Kuboi, S.; Kato, H.; Seki, Y.; Suzuki, H.; Toyoda, H. Mass Spectroscopic Measurement of Time-Varying Ion Composition in a Pulse-Modulated $Ar/C_4F_8/O_2$ Dual-Frequency Capacitively Coupled Plasma. *Jpn. J. Appl. Phys.* **2023**, *62*, SI1003. [CrossRef]
29. Chesaux, M.; Howling, A.A.; Hollenstein, C. Funnelling of Rf Current via a Plasmoid through a Grid Hole in an Rf Capacitive Plasma Reactor. *Plasma Sources Sci. Technol.* **2013**, *22*, 055006. [CrossRef]
30. Kim, Y.; Lee, H.; Chang, H. Micro-Arc Ignition on the Oily Surface of Capacitively-Coupled Plasma. *Curr. Appl. Phys.* **2015**, *15*, 313–318. [CrossRef]
31. Stefanović, I.; Sadeghi, N.; Winter, J.; Sikimić, B. Influence of Nanoparticle Formation on the Time and the Space Resolved Metastable Density in Argon-Acetylene Plasmas. *Plasma Sources Sci. Technol.* **2017**, *26*, 065014. [CrossRef]
32. Ogawa, D.; Chung, C.W.; Goeckner, M.; Overzet, L. Transient Effects Caused by Pulsed Gas and Liquid Injections into Low Pressure Plasmas. *Plasma Sources Sci. Technol.* **2010**, *19*, 034013. [CrossRef]
33. Sackers, M.; Busch, C.; Tsankov, T.V.; Czarnetzki, U.; Mertens, P.; Marchuk, O. Plasma Parameters and Tungsten Sputter Rates in a High-Frequency CCP. *Phys. Plasmas* **2022**, *29*, 043511. [CrossRef]

Disclaimer/Publisher's Note: The statements, opinions and data contained in all publications are solely those of the individual author(s) and contributor(s) and not of MDPI and/or the editor(s). MDPI and/or the editor(s) disclaim responsibility for any injury to people or property resulting from any ideas, methods, instructions or products referred to in the content.